Journal of African Earth Sciences 58 (2010) 457–474

Contents lists available at ScienceDirect

Journal of African Earth Sciences

journal homepage: www.elsevier.com/locate/jafrearsci

Evolution of Cu–Co mineralizing fluids at Nkana Mine, Central African Copperbelt, Zambia

Ph. Muchez [a,*], D. Brems [a], E. Clara [a], A. De Cleyn [a], L. Lammens [a], A. Boyce [b], D. De Muynck [c,d], W. Mukumba [e], O. Sikazwe [f]

[a] Geodynamics and Geofluids Research Group, Department of Earth and Environmental Sciences, K.U. Leuven, Celestijnenlaan 200E, B-3001 Leuven, Belgium
[b] Scottish Universities Environmental Research Centre, Rankin Avenue, Scottish Enterprise Technology Park, East Kilbride G75 0QF Scotland, UK
[c] Center for Archaeological Sciences, Department of Earth and Environmental Sciences, K.U. Leuven, Celestijnenlaan 200E, B-3001 Leuven, Belgium
[d] Department of Analytical Chemistry, Ghent University, Krijgslaan 281-S12, B-9000 Ghent, Belgium
[e] Mopani Copper Mines Plc., Nkana Mine Site, P.O. Box 22000, Kitwe, Zambia
[f] University of Zambia, School of Mines, Geology Department, P.O. Box 32379, Lusaka, Zambia

ARTICLE INFO

Article history:
Received 7 October 2009
Received in revised form 4 May 2010
Accepted 10 May 2010
Available online 19 May 2010

Keywords:
Nkana
Zambian Copperbelt
Sediment-hosted Cu–Co deposits
Fluid inclusions
Stable isotopes
Sr isotopes

ABSTRACT

The Central African Copperbelt hosts numerous world class stratiform Cu–Co deposits in the Neoproterozoic Katanga Supergroup (<880 to ± 500 Ma). These high grade deposits resulted from multiple mineralization and remobilization stages. The Nkana Cu–Co deposit in the Zambian part of the Copperbelt is such a stratiform deposit but the location of the rich ore bodies is structurally controlled, i.e. occurring in the hinge zones of tight to isoclinal folds. Late stage mineralization and/or remobilization caused this enrichment. Three major mineralization/remobilization stages have taken place during the Lufilian orogeny. They are characterized by folded layer parallel veins, highly irregular veins crosscutting the folds, and finally unfolded massive veins.

An evolution in the oxygen, carbon and sulphur isotopic composition is present from the layer parallel and irregular to the massive veins. The more negative $\delta^{18}O$ values in the carbonates from the massive veins most likely reflect a decrease in the oxygen isotopic composition of the ambient, metamorphic fluids. The $\delta^{13}C$ values range between −25‰ and −5‰ V-PDB with a trend towards less negative values in the massive veins, possibly reflecting an ongoing oxidation of organic matter in a relatively closed system. Early framboidal and massive pyrites disseminated in the host rock have distinctly negative $\delta^{34}S$ values, i.e. between −16‰ and −9.7‰ V-CDT. The sulphur isotopic composition increases from these early diagenetic pyrites to sulphides in the successive vein generations. The $\delta^{34}S$ values of the massive veins are positive and cluster between 1.3‰ and 2.0‰ V-CDT. This enrichment in heavy sulphur is interpreted as a result of the mixing of S remobilized from early sulphides, with S derived from the thermochemical reduction of sulphate. With time, the sulphur derived from TSR became more important. The Sr isotopic composition of the carbonates in all three vein generations shows a wide range between 0.71672 and 0.75407. All values are significantly more radiogenic than the strontium isotopic composition of Neoproterozoic marine carbonates (0.7056–0.7087). The radiogenic values indicate interaction of the mineralizing fluid with the basement or the siliciclastic sediments derived from it. All fluid inclusions measured in the different vein generations have a dominant H_2O–NaCl/KCl–$MgCl_2$ composition with the presence of a gaseous component in some inclusions. Fluid inclusions in the layer parallel veins suggest entrapment around 450 °C at a depth of 8.4 km (2100 bars), i.e. during the main period of metamorphism. Secondary fluid inclusions of unknown origin in the layer parallel, irregular and massive veins have a high salinity (18.1 to >23.2 eq. wt.% NaCl) and homogenization temperatures between 100 and 250 °C. These fluids were trapped after formation of the veins, likely during retrograde metamorphism.

The study of the veins, which formed between 580 and 520 Ma, nicely demonstrate the complexity of the metallogenesis of the Cu–Co ore deposits in the Copperbelt. Therefore, geochemical, microthermometric and geochronological analyses need to be carried out on individual generations to fully understand the evolution of ore formation through time.

* Corresponding author. Tel.: +32 16 327584; fax: +32 16 327981.
E-mail address: philippe.muchez@ees.kuleuven.be (Ph. Muchez).

1464-343X/$ - see front matter © 2010 Elsevier Ltd. All rights reserved.
doi:10.1016/j.jafrearsci.2010.05.003

1. Introduction

Several metallogenic models have been proposed for the origin of the stratiform Cu–Co deposits in the Copperbelt, central Africa. Initially an epigenetic-magmatic origin was proposed (Jackson, 1932), which was followed in time by the syn-sedimentary model for the Zambian Copperbelt (Garlick, 1964; Fleischer et al., 1976). A syn-sedimentary origin was questioned by Annels (1974) and Bartholomé (1974), who both clearly demonstrated the replacive nature of the Cu–Co sulphides and thus their diagenetic origin. Although a pre-orogenic origin was accepted by many researchers, the discussion continued on the early versus late diagenetic origin of ore formation (see Haynes, 1986). Subsequent petrographic, isotopic (C, O, S) and microthermometric studies aimed to specify the sulphur and even the metal source, and the temperature and origin of the mineralizing fluid (Annels, 1989; Sweeney and Binda, 1989). During diagenesis, bacterial reduction of Neoproterozoic seawater sulphate and evaporates present in nodules formed the sulphur source (Dechow and Jensen, 1965; Lerouge et al., 2005; Muchez et al., 2008). Copper and cobalt are thought to have been mainly leached from the basement during crustal rifting (Annels and Simmonds, 1984). Hydrothermal fluids migrated along basement fractures and faults into the overlying Katangan rocks (Annels, 1989). The importance of remobilization of the pre-orogenic ores during metamorphism and the Lufilian orogeny was already recognized in early studies (Bard and Jordaan, 1963). McGowan et al. (2003, 2006) proposed a syn-orogenic origin for the Nchanga ore deposit based on a combination of structural, petrographic and isotopic criteria.

Recently, consensus is reached in literature that the high grade Cu–Co deposits resulted from multiple mineralizing stages (Cailteux et al., 2005; Selley et al., 2005; Dewaele et al., 2006; El Desouky et al., 2009a). Mineralization started during early diagenesis and was followed by a major second phase during late burial and the Lufilian orogeny. Based on an extensive study of numerous large ore deposits in the Zambian Copperbelt and a review of the literature, Selley et al. (2005) concluded that three significant tectonic phases affected the basin. Firstly, extension associated with early rifting led to syn-sedimentary faulting and fault-controlled basins. The connection of these small basins occurred during sedimentation of the most important host rock of the ores. The early diagenetic mineralization phase is interpreted to have occurred during this rifting period (Muchez et al., 2007). Secondly, a later period of extension occurred at ~765–735 Ma, which led to the development of a proto-oceanic rift, comparable to the Red Sea (see Kampunzu et al., 1991) with limited mafic magmatism (Kampunzu et al., 2000). No distinct Cu–Co mineralization phase in the Lower Roan rocks has been associated with this period, however, mineralization within the Upper Roan rocks could be associated with this phase (El Desouky, pers. comm. 2010). Finally, basin inversion and compressional tectonics (Selley et al., 2005) caused remobilization of the pre-existing ore and could have led to a supply of metals. The latter forms a topic for further research.

In the Zambian Copperbelt, clear petrographic evidence for the first, early diagenetic phase is often lacking, forming the base for the discussion on the early diagenetic versus late burial (up to metamorphic) origin of ore deposition. This could be due to its absence or, more likely, to the higher metamorphic grades in the Zambian Copperbelt, which obliterated the first mineralization phase due to complete remobilization. Although the remobilization phase has been recognized for many decades (e.g. Garlick, 1961, 1964), the distinction between the different phases in geochemical studies has only recently been made in the Democratic Republic of Congo (DRC; El Desouky et al., 2009a, accepted for publication) and not in Zambia. Greyling et al. (2005) distinguished different phases in their detailed microthermometric study of fluid inclusions in gangue minerals from a mineralized, lateral secretion bedding parallel quartz vein at Chambishi. The second major, late burial to syn-orogenic mineralization phase likely consists of several subphases (El Desouky et al., 2009a). Brems et al. (2009) distinguished three main subphases at Nkana which range from the onset of orogenic compression around 585 Ma until late orogenesis at 525 Ma.

The aim of this study is to determine the evolution in the chemistry of the mineralizing/remobilizing fluids from the onset of orogenesis and metamorphism until late to post-orogenic conditions, based on a geochemical and microthermometric study of the different mineralization stages at Nkana.

2. Geological setting

The Zambian Copperbelt forms part of the arc-shaped Lufilian belt, which extends from Zambia into the Katanga Province in the DRC (Fig. 1). In Zambia, the belt extends in northwest–southeast direction, with the Kafue Anticline as a prominent northwest–southeast oriented, northwest plunging structural feature controlling the ore deposits. These are located both southwest (e.g. Konkola, Nchanga, Nkana) and northeast (e.g. Mufulira) of the anticline (Fig. 1).

The Lufilian belt is a 700 km long and 150 km wide northerly oriented fold and thrust belt between the Congo and Kalahari Cratons (Selley et al., 2005). This belt formed due to Neoproterozoic extensional tectonics during the break-up of supercontinent Rodinia and the late Neoproterozoic to early Phanerozoic collision, deformation and metamorphism. The Lufilian fold belt consists of four distinct zones, all exhibiting a different deformation style (Porada, 1989; Kampunzu and Cailteux, 1999; Porada and Berhorst, 2000). From north to south, these are the External fold and thrust belt, the Domes region, the Synclinorial belt and the Katanga high. The Katangan Copperbelt occurs within the External fold and thrust belt. The Zambian Copperbelt is situated within the Domes region. These two zones are characterized by a different metamorphic grade, evolving from zeolite and greenschist facies in the External fold and thrust belt to greenschist and amphibolite facies in the Zambian Domes region (Mendelsohn, 1961; Key et al., 2001). The External fold and thrust belt comprises a thin-skinned geometry with complex macroscale fragmentation and thrust repetition of the Katanga Supergroup stratigraphy. In the Domes region, Katanga Supergroup strata unconformably overlie the basement and are deformed together with the basement units. The structural style is dominated by upright to inclined, high-amplitude folds (Selley et al., 2005). Basement inliers in the Domes region are thought to represent antiformal stacks above mid to lower crustal ramps, indicating a thick-skinned deformation (Daly et al., 1984).

The Katanga Supergroup was deposited during the Neoproterozoic era. The Nchanga Red Granite (883 ± 10 Ma; Armstrong et al., 2005) is intrusive in the Palaeoproterozoic basement rocks and is unconformably overlain by the first Katanga Supergroup sediments. The Katanga Supergroup is subdivided into the Roan, Nguba and Kundelungu Groups (Fig. 2; Cailteux et al., 2005, 2007). Wendorff (2002, 2005) proposed an alternative tectonostratigraphic subdivision of this supergroup into the Roan, Guba, Kundelungu and Fungurume Groups. The focus of this paper, the Roan Group, is similar in both subdivisions. The Roan Group is made up of siliciclastics, carbonate rocks and plutonic rocks emplaced in a continental rift (Porada and Berhorst, 2000).

In Zambia, the Roan Group is subdivided into the Mindola, Kitwe, Kirilabombwe and Mwashia Subgroups. The Mindola Subgroup consists of texturally immature conglomerates and subarkosic sandstones that are deposited in fluvial, alluvial fan, aeolian and

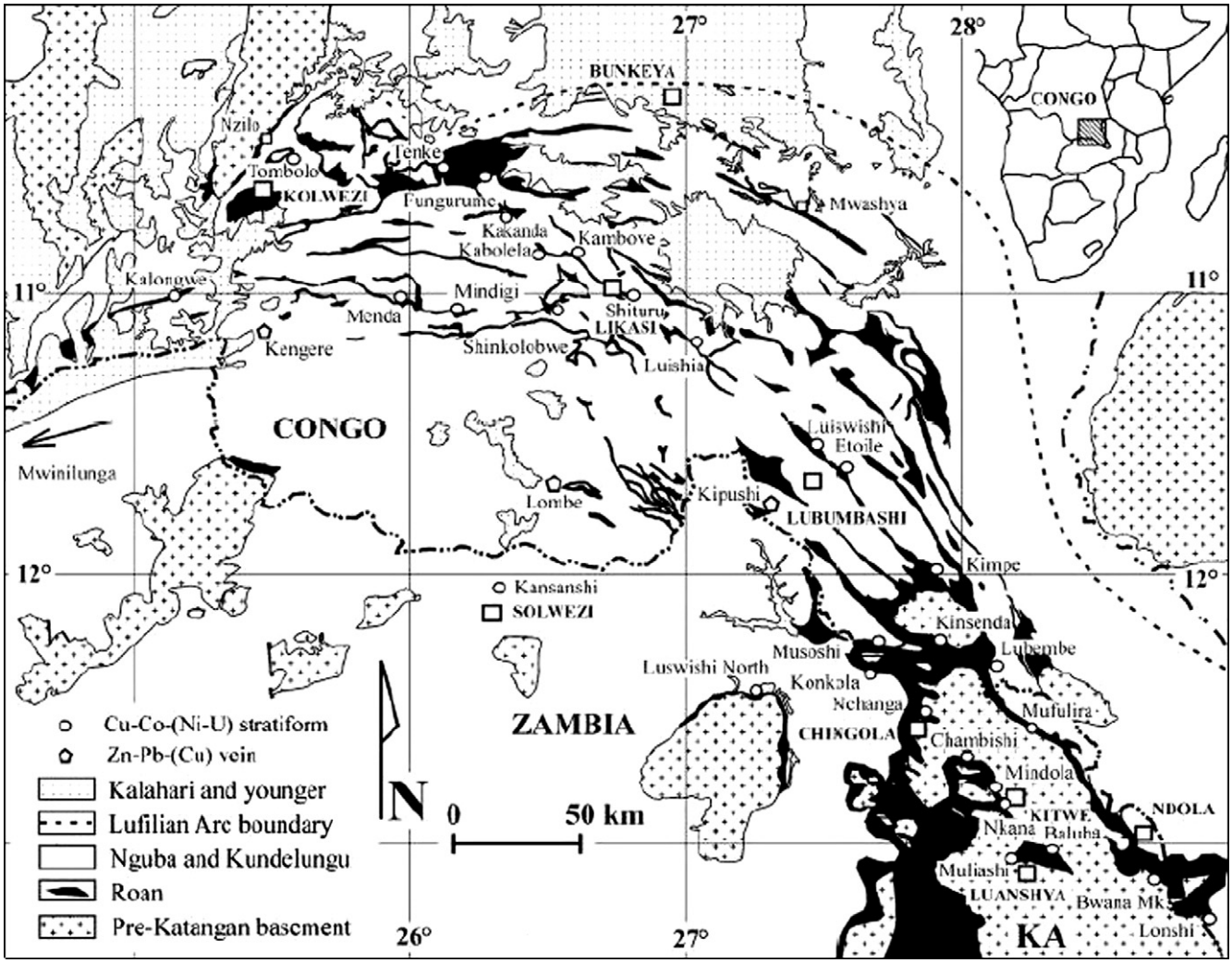

Fig. 1. Location of the Central African Copperbelt and the most important ore deposits (after Cailteux et al., 2005).

fan-delta environments and is characterized by significant lateral and vertical facies variations (Jordaan, 1961). The sediments were deposited in narrow troughs or subbasins bounded by basement cored topographic highs (Selley et al., 2005). At its base, the Kitwe Subgroup hosts the Ore Shale Formation, which contains the main Cu–Co mineralizations. It includes a succession of arenites, silty to sandy arenites and shales northeast of the Kafue Anticline and dolomitic shales and dolomites southwest of this anticline. The sediments represent a transgressive succession deposited in an evaporitic environment (Garlick, 1961; Binda and Mulgrew, 1974; Unrug, 1988). The overlying Kirilabombwe Subgroup contains dolomites and arenitic dolomites interbedded with dolomitic shales. Interbedded gabbros occur, having a mafic to intermediate composition. They are dated at an age of 760 ± 5 Ma (Key et al., 2001). The overlying Mwashia Subgroup consists of platform carbonates in the lower part and more open marine dolomitic shales, black shales and quartzites in the upper part. A glacial diamictite, the Grand Conglomerate, forms the base of the Nguba Group (Cailteux et al., 2005). It is correlated with Sturtian diamictites deposited at approximately 740 Ma (e.g. Hoffman et al., 1998; Fanning and Link, 2004). The Nguba assemblage is composed of siliciclastics, carbonates and mafic igneous rocks emplaced in a proto-ocean similar to the Red Sea (Kampunzu et al., 1991). The Kundelungu starts with a second diamictite, i.e. the Petit Conglomerate. Further sedimentation consists of carbonates, siltstones and mudstones (Selley et al., 2005). These deposits represent syn- to post-orogenic continental molasse, which continued into the early Palaeozoic (Kampunzu and Cailteux, 1999; Cailteux et al., 2005). During the Lufilian orogeny, the Katanga basin closed and the sediments underwent deformation and metamorphism (Kampunzu and Cailteux, 1999; Porada and Berhorst, 2000).

3. The Nkana ore deposit

The Nkana copper–cobalt deposit occurs in a northwesterly plunging syncline (Nkana Syncline) at the southeastern end of the Chambishi–Nkana basin (Jordaan, 1961; Bard and Jordaan, 1963). This basin lies on the southwestern flank of the Kafue Anticline and is elongated in a northwesterly direction (Fig. 3). Only the northeastern limb of the Nkana syncline is economically mineralized. The mining area has a combined strike length of ~14 km, of which ~12.5 km contains economic Cu mineralization (Bard and Jordaan, 1963; Croaker et al., 2003). Central and South Orebody at Nkana are separated from the Mindola area by the Kitwe barren gap (Jordaan, 1961), recognized as a biohermal dolomite reef on top of a granite hill (Annels, 1974; Binda and Mulgrew, 1974; Clemmey, 1974; Garlick and Fleischer, 1972). The oldest rocks at Nkana belong to the Lufubu Metamorphic Complex and consist of mica schist, gneisses and quartzites of Precambrian age. The

Era		Group	Subgroup	Formation	Lithologies
Paleozoic	± 500 Ma	Kundelungu	Biano Ku3		Arkoses, conglomerates, argillaceous sandstones
			Ngule Ku 2	Sampwe Kiubo Mongwe	Dolomitic pelites, argillaceous to sandy siltstones Dolomitic sandstones, siltstones and pelites Dolomitic pelites, siltstones and sandstones
Neoproterozoic			Gombela Ku 1	Lubudi Kanianga Lusele Kyandamu	Pink oolitic limestone and sandy carbonate beds Carbonate siltstones and shales Pink to grey micritic dolomite "Petit Conglomérat": glacial diamictite
	± 620 Ma	Nguba	Bunkeya Ng 2	Monwezi Katete	Dolomitic sandstones, siltstones and pelites Dolomitic sandstones, siltstones and shales in northern areas; alternating shale and dolomite beds in southern areas.
			Muombe Ng 1	Kipushi Kakontwe Kaponda Mwale	Dolomite with dolomitic shale beds in southern areas Carbonates Carbonate shales and siltstones; "dolomite Tigrée" at the base "Grand Conglomérat": glacial diamictite
	± 750 Ma	Roan	Mwashya		Dolomitic shales, grey to black carbonaceous shales, quartzites
			Kirilabombwe	Kanwangungu Kibalongo	Dolomites to arenitic dolomites interbedded with dolomitic shales; intrusive gabbros Slates with grit (Antelope Clastics)
			Kitwe	Chingola Pelito-Arkosic Ore Shale	Dolomites, argillite beds at top Arkoses, sandy to dolomitic argillites Arenites, argillaceous dolomites, argillites, dolomites, evaporites ; Main stratiform Cu-Co mineralisation in the lower part
			Mindola	Mutonda Kafufya Chimfunsi	Conglomerates, coarse arkoses and argillaceous siltstones Quartzites Pebble and cobble conglomerate
	≤ 880 Ma				

Fig. 2. Lithostratigraphy of the Zambian deposits of the Katanga Supergroup (after Cailteux et al., 2005, 2007).

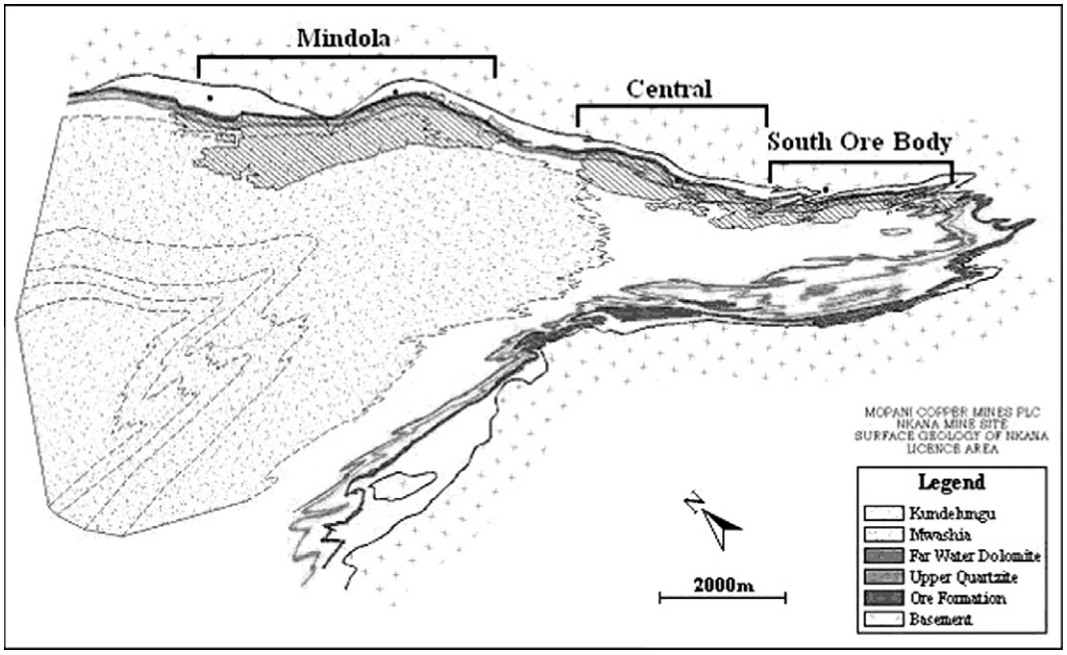

Fig. 3. Nkana Syncline with the location of the Nkana South, Nkana Central and Mindola Orebodies.

mica schists are well foliated, grey to black and may show a wide range in grain sizes. The gneisses and schists immediately below the Footwall Orebody are mineralized by chalcopyrite and bornite.

The Mindola Subgroup is subdivided into three lithostratigraphic units (Fig. 4): the Basal Conglomerate, the Basal Quartzite and the Footwall Sandstone. The Basal Conglomerate was deposited in valleys and on the flatter slopes of the uneven pre-Katanga surface (Jordaan, 1961). The Basal Quartzite consists of white, feldspathic, rather massive argillaceous quartzites. The Footwall Sandstone is composed of interbedded arkoses, feldspathic and dolomitic sandstones and thin argillites. The Lower Conglomerate, present at the base of the Footwall Sandstone (Fig. 4), consists of rounded to sub-rounded pebble to cobble-sized fragments of granite, quartzite, vein quartz and schist within medium- to coarse-grained feldspathic to argillaceous sandstone. The Footwall Conglomerate at the top of the Footwall Sandstone (Fig. 4),

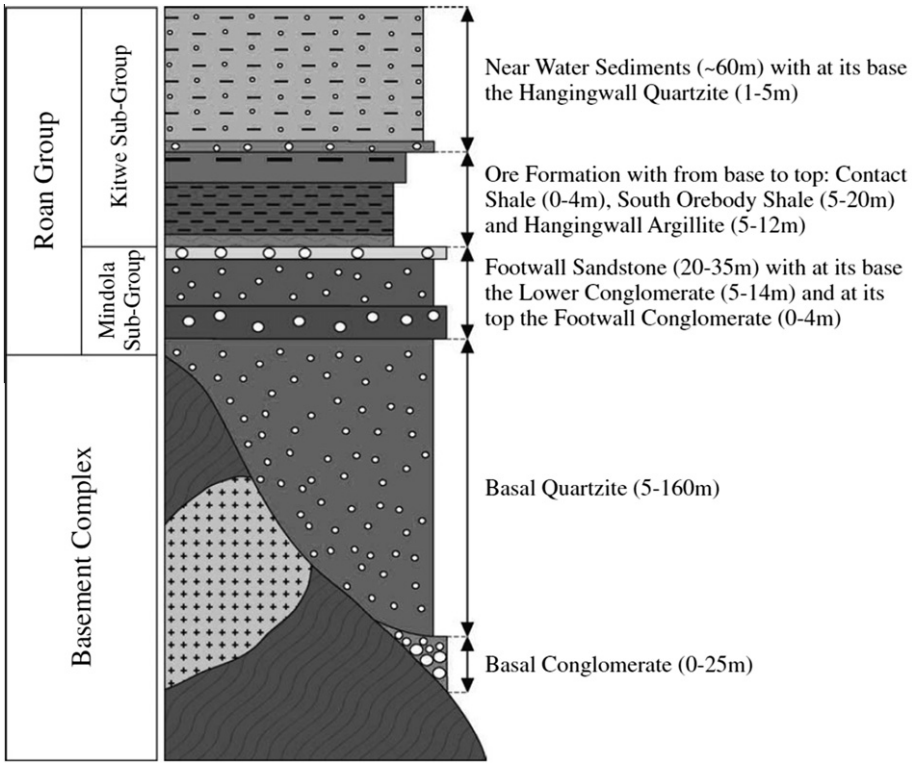

Fig. 4. Schematic lithostratigraphical column of the lower part of the Roan Group at Nkana (after Brems et al., 2009).

consists of angular to rounded fragments of quartz, dark quartzite, schist and granite set in an arkosic to feldspathic, sandy, clayey or more siliceous matrix (Jordaan, 1961).

The Kitwe Subgroup comprises the rocks of the former Musoshi Subgroup (Clemmey, 1974; Cailteux et al., 2005). The two major lithostratigraphic units are the Ore Shale and the Near Water Sediments (Fig. 4). The Ore Shale comprises the South Orebody (SOB) Shale at its base and the Hanging Wall Argillite at its top. At South Orebody, the Ore Shale consists of a black carbonaceous shale underlain by a thin red-grey dolomitic shale. This succession grades laterally (from Nkana Central Orebody to Mindola) into a zone composed of micaceous shale and tremolite schist followed by argillites and impure dolomites (Bard and Jordaan, 1963). At the base of the South Orebody Shale, an alteration zone is present. This Contact Shale has a highly variable thickness (0–4 m) and has no stratigraphical significance (Brems et al., 2009). The alteration resulted in a composition ranging from a tremolitic shale or schist to a dense, silicified argillite. The Hanging Wall Argillite is composed of a dark grey to greenish grey argillite showing thick banding (Jordaan, 1961). The Near Water Sediments exhibit a highly silicified unit at the base, i.e. the Hanging Wall Quartzite. The Near Water Sediments further comprise a ~60 m thick sequence consisting of interbedded, medium-grained brown and grey feldspathic sandstones, thinly banded, grey to greenish argillites and dolomitic argillites, a few light grey to almost white medium-grained feldspathic quartzites and brownish well-bedded dolomites.

After deposition of the Katanga Supergroup, the Lufilian deformation produced the dominant structural pattern of the Copperbelt. The intensity of this deformation varied over the extent of the Nkana Syncline (Bard and Jordaan, 1963). The Nkana Syncline is a northwest-plunging asymmetrical syncline with the axial plane dipping to the northeast. The northeastern limb of the syncline is steep to vertical and locally overturned (Jordaan, 1961). The intensity of deformation increases towards the nose and subsidiary folds range from open to isoclinal (Bard and Jordaan, 1963; Brems et al., 2009). Tight to isoclinal folding, double plunging folds, curved axial planes, low angle shears and hinge zone thickening characterize the deformation observed in the Ore Shale (Croaker et al., 2003; Brems et al., 2009). Hinge zone thickening is particularly important in the more folded areas where the distribution of the ore suggests remobilization as a result of folding (Bard and Jordaan, 1963). According to Bard and Jordaan (1963), no relation exists between the copper concentrations and faulting or fracturing.

The metamorphic assemblage of biotite, chlorite, tremolite, talc, sericite and albite in the Ore Shale Formation indicates a greenschist metamorphic facies. There is some variation in grade from the quartz-albite-epidote-biotite subfacies in the more highly deformed areas to the quartz-albite-muscovite-chlorite subfacies in the less deformed rocks. Fibrous aggregates and prismatic and acicular crystals of tremolite are formed in the more carbonaceous and folded beds of the Ore Shale. It is particularly abundant at the base of the Ore Shale, close to the contact with the Footwall Conglomerate. In the quartzitic rocks, metamorphic recrystallization did not destroy the sedimentary macro- and microstructures.

The majority of the deposits in the Zambian Copperbelt occur close to the basement domes, the most important one being the Kafue Anticline, along which also the Nkana mine occurs (Garlick, 1961). At Nkana Southern Orebody, minor economic mineralization occurs in the arenites and conglomerates of the Mindola Subgroup, i.e. the Nkana Footwall Orebody (Binda and Mulgrew, 1974). Most of the copper sulphides are present within the Ore Shale Formation, which ranges from a black carbonaceous shale in the southeast (Nkana Southern Orebody) to an argillite and dolomite assemblage in the north-west (Mindola deposit; Bard and Jordaan, 1963). High grade mineralization is only found along the northeastern limb of the Nkana Syncline (Jordaan, 1961). Mineralized veins are abundant within Central Orebody. Several generations of veins including bedding parallel and crosscutting veins are

common in highly deformed parts of the orebody (Jordaan, 1961; Brems et al., 2009). All vein sets carry copper sulphides to different degrees (Bard and Jordaan, 1963). Sulphide remobilization related to deformation and metamorphism has resulted in thick, high grade zones at fold hinges and small ore shoots crosscutting stratigraphy (Croaker et al., 2003; Brems et al., 2009). The main ore minerals at the Nkana deposit are chalcopyrite, bornite and carrolite (Jordaan, 1961). Pyrite often occurs in association with the chalcopyrite. Other copper minerals present include chalcosite, native copper, and in the near surface zone, a range of copper carbonates, phosphates and silicates (Clemmey, 1974).

4. Petrography and paragenetic sequence

4.1. Results

A petrographic study was carried out on samples taken from borehole NS0168 at Nkana South Orebody and from boreholes CE 570 and CE 555 at Nkana Central Orebody. Borehole NS0168 is a 400.5 m long horizontal borehole and was drilled in northeastern direction, largely perpendicular to the strata. The starting coordinates were 12°51′5.072″S, 28°11′51.460″E and 246.70 m above sea level (Nkana South Orebody). Borehole CE 570 was drilled almost horizontal (inclination +2°), with starting coordinates 12°49′43.413″S, 28°11′27.846″E and 113.95 m above sea level, and with an azimuth of 270° (Nkana Central Orebody). The total length of the borehole is 484 m. Borehole CE 555 was also drilled nearly horizontal (inclination +4.2°), with the same starting coordinates and at the same depth as borehole as borehole CE 570, and an azimuth of 281.84°. The total length is 292.5 m. The results from the petrographic study of borehole NS0168 were published by Brems et al. (2009). In addition to disseminated sulphide minerals, they distinguished three main vein generations, i.e. layer parallel veins, irregular veins and massive veins. The summary below is based on the work of Brems et al. (2009) and Lammens (2009) and complemented with the data from the two boreholes from Nkana Central Orebody studied by De Cleyn (2009). Disseminated sulphides include pyrite, chalcopyrite, bornite and pyrrhotite. These sulphides may be stretched along the cleavage planes.

Characteristic in the boreholes CE 555 and 570 is the presence of lenticular nodules in the SOB Shale and in the Hanging Wall Argillite. They range in size from a millimetre up to a few centimetres and consist of biotite, chlorite, muscovite, quartz, carbonate and sulphides (Fig. 5A). They are somewhat flattened and have pressure shadows along the cleavage direction, where the nodules pinch out in elongated tips. Within the pressure shadows, fine-grained muscovite, biotite, quartz and iron-rich calcite with abundant twinning are present. More coarse-grained muscovite and biotite occur along the edges of the nodules. These crystals are aligned parallel to the nodule and are sometimes bent. Within the nodules, pyrite cubes commonly occur along the edges (Fig. 5B) and precipitated before biotite, chlorite, muscovite, quartz and carbonates. Sometimes, pyrite may occur throughout the whole nodule. Quartz formed after pyrite, but before carbonate, which fills the centre of the nodule (Fig. 5C). They show a free-growing texture. Within the nodules, some relicts of anhydrite may be present (Fig. 5C). In addition to pyrite, other sulphides occur, especially in the pressure shadows. Chalcopyrite overgrows and replaces pyrite. Pyrrhotite is often associated with chalcopyrite and forms irregularly shaped masses. It can replace euhedral pyrite and contains lamellar to flame-like exsolutions of pentlandite. Millimetre-sized nodules, consisting almost entirely of sulphides, also occur.

The layer parallel veins comprise veins that occur (sub)parallel to bedding and have a width from less than a millimetre up to a few centimetres (Fig. 6A). They contain anhedral, subhedral to euhedral pyrite, chalcopyrite, pyrrhotite, bornite and pentlandite as sulphides, and iron-rich carbonates, quartz, muscovite and biotite as gangue minerals. Biotite and muscovite are often oriented along the length direction of the vein. Pyrite is often partly replaced by chalcopyrite and pyrrhotite. Both latter minerals also occur as irregular and massive crystals, sometimes overgrowing pyrite (Fig. 5D). The layer parallel veins are often deformed with the gangue and especially the ore minerals stretched along cleavage planes. Biotite may be altered to chlorite. In the altered zones, rosettes of tremolite are present, which affects both the host rock and the vein filling cements. Therefore, tremolitization clearly postdates the vein-filling minerals. The layer parallel veins are often folded and fractured (Fig. 6B). The same gangue and ore minerals as in these fractures are concentrated in the hinge zones of the folds (Fig. 6C and D).

Irregular veins crosscut the folds and the cleavage (Fig. 6E). They may contain relicts of the host rock. The veins are filled with quartz, carbonate, microcline, muscovite, biotite, pyrite, chalcopyrite, bornite, pyrrhotite and chalcocite. The micas precipitated first and occur along the edges of the veins. They are surrounded by quartz, carbonates and sulphides. Quartz may contain tiny sulphide inclusions but usually it represents an early phase in the veins that is surrounded by carbonates and sulphides. The carbonates are often the latest phase and enclose the micas, quartz and sulphides. Chalcopyrite is the most important Cu-sulphide and may replace earlier formed pyrite. Bornite sometimes shows exsolution lamellae of chalcopyrite. Chalcocite is rare and is present along the margins of chalcopyrite and bornite crystals.

Unfolded massive veins crosscut the stratification, the layer parallel and irregular veins (Fig. 6F). They consist of iron-rich calcite, quartz, muscovite, biotite, feldspar, anhydrite, chalcopyrite, pyrrhotite, bornite, carrolite, pyrite, molybdenite and pentlandite. Occasionally amphibole (hornblende) and clinopyroxene (diopside) are present. The calcite and quartz minerals range between a few millimetres up to a few centimetres. Chalcopyrite is abundant as massive, irregular masses. Pyrrhotite shows lamellar exsolution flames of pentlandite and may occur intertwined with chalcopyrite. Pyrite is rare in the massive veins and is overgrown by chalcopyrite and pyrrhotite. Sometimes, the calcite shows a bright fuchsia colour, characteristic for a cobalt-bearing calcite. Strongly pleochroic and an isotropic molybdenite crystals are present in these veins.

4.2. Interpretation

The relative time relationship between the disseminated Cu-sulphides and the veins can not be specified. The nodules, filled with quartz, carbonates, micas and sulphides with some relicts of anhydrite, are comparable to the pseudomorphosed anhydrite nodules, which occur abundantly in the Copperbelt (Cailteux, 1994; Lefebvre, 1978; Muchez et al., 2008; El Desouky et al., 2009a). According to Brems et al. (2009), the layer parallel veins formed during the initial phase of basin inversion. The formation of prefolding, layer parallel veins requires extensional forces perpendicular to the bedding. Even though this can be caused by lithostatic fluid overpressures applicable during sediment burial, this type of overpressure is reached more easily when compressive tectonic stresses are superimposed on the system (Sibson, 2001; Cobbold and Rodrigues, 2007). The layer parallel veins at Nkana are interpreted to postdate burial diagenesis and are linked to supralithostatic pressures generated in a compressive stress regime at the onset of the Lufilian orogeny (Brems et al., 2009). During further compression, the rocks and the layer parallel veins were folded, with a concentration of ore and gangue minerals in the hinge zones of the folds. The highly irregular veins, which may

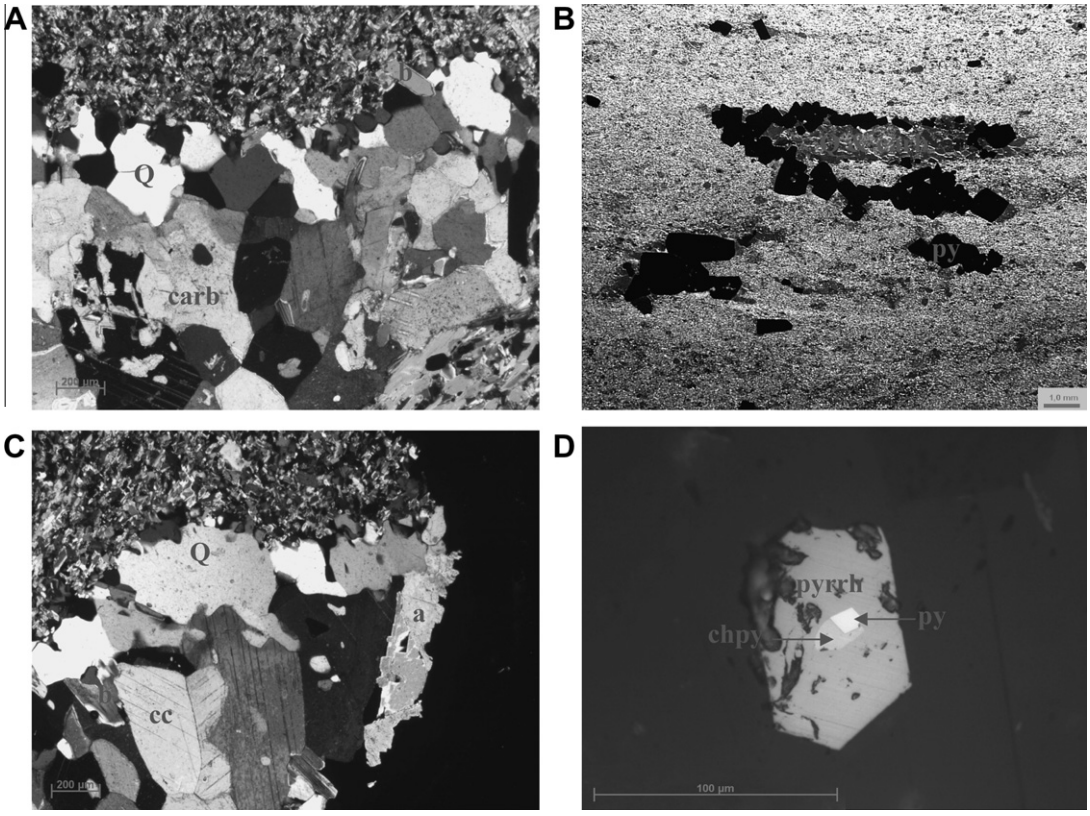

Fig. 5. (A) Nodule within fine-grained matrix. The nodule consists of quartz (Q) along its edge and carbonates (carb) are present in the centre. Borehole CE570, transmitted light, crossed nicols. (B) Sub- to euhedral pyrite crystals (py) along the edge of a nodule. Smaller nodules are almost completely filled with pyrite. The larger nodule also contains quartz and carbonate. Borehole CE570, binocular transmitted light. (C) Fine-grained matrix with nodule dominantly composed of quartz (Q), carbonates (cc) and anhydrite (a). Borehole CE570, transmitted light, crossed nicols. (D) Pyrite (py) overgrown by chalcopyrite (chpy) and pyrrhotite (pyrrho). Borehole CE570, plane polarized reflected light.

be connected to these hinge zones and contain rock fragments, likely formed at high fluid pressures (cf. Sibson, 2001). A five point Re–Os isochron with analyses of disseminated and vein-type sulphides of the Nkana, Chibulumba and Nchanga ore deposits yielded an age of 583 ± 24 Ma (Barra et al., 2004). This age corresponds to the onset of metamorphism and the orogeny (Rainaud et al., 2005), and thus likely represents the deformation phase related to the layer parallel phase or early orogenic mineralization phase as defined by Greyling et al. (2005) in the Zambian Copperbelt.

The massive veins are not folded. They crosscut the stratification, the layer parallel and the irregular veins. They contain molybdenite and pervasive anhydrite that have not been recorded in the earlier vein generations. Their presence could indicate that a new fluid phase was responsible for the mineralization of the massive veins. Indeed, a much younger Re–Os age of 525.7 ± 3.4 Ma has been recorded from the molybdenite in these veins at Nkana by Barra et al. (2004).

5. Fluid inclusion microthermometry

5.1. Results

Fluid inclusions were investigated in quartz from the three main vein generations. Inclusions occurring in distinct growth zones are interpreted as primary, while inclusions present in trails are said to be secondary inclusions (Goldstein and Reynolds, 1994). Inclusions that can not be attributed to one of both groups are classified as being of unknown origin. The size of the inclusions measured ranges between 4 and 30 μm and all inclusions are two-phase at room temperature.

Three fluid inclusion assemblages have been studied in the layer parallel veins. One assemblage represents secondary inclusions and the two other are of unknown origin. The microthermometric data of the melting temperatures is mostly similar in the three assemblages, but different homogenization temperatures were measured. During cooling, the inclusions become completely frozen between −60 and −47 °C. In three inclusions of unknown origin, a solid phase forms around the vapor bubble between −49 and −36 °C, indicating the formation of clathrate. During reheating, first melting has been observed between −26 and −17 °C. Final melting of ice varies between −16.4 and −5.4 °C (Fig. 7). No second liquid phase, e.g. of CO_2, has been observed. Final dissociation of clathrate in the three inclusions mentioned above is between 3.3 and 7.6 °C. Homogenization to the liquid phase of the inclusions of unknown origin occurred between 203 and 270 °C, except for one value of 130 °C. The homogenization temperature of the secondary inclusions lies between 138 and 151 °C (Fig. 8).

Two fluid inclusion assemblages have been studied in the irregular veins and these are both of unknown origin. The vapor bubble occupies 5–10% of the inclusion. Freezing temperatures range between −71 and −55 °C. First melting is observed between −28 and −24 °C and the final melting of ice occurs between −24.1 and −18.2 °C (Fig. 9). Homogenization into the liquid phase occurs between 92 and 157 °C (Fig. 10).

Two fluid inclusion assemblages have been studied in quartz from a massive vein. One assemblage occurs in a trail and the origin of the second is unknown. No difference in microthermometric

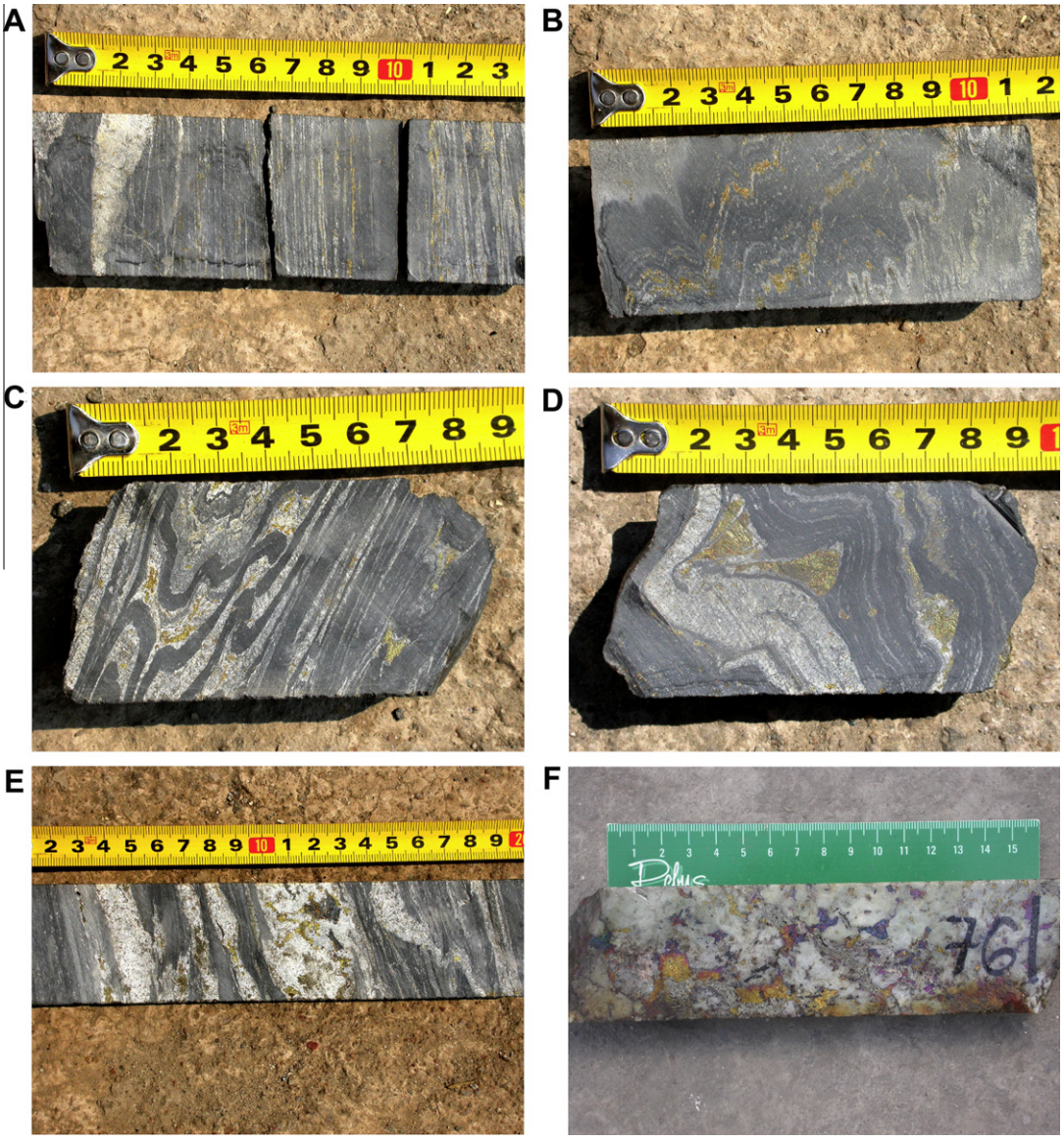

Fig. 6. (A) Dark grey shale with layer parallel veins with calcite, dolomite, quartz, chalcopyrite and pyrite. In the left part of the photograph, the shale is crosscut by several irregular veins. Borehole NS0168. (B) Intensely folded rock consisting of dark grey shale and layer parallel carbonate veins with chalcopyrite and pyrite. Borehole NS0168. (C) Dark grey shale with intensely folded and fractured carbonate veins with chalcopyrite, with concentration of ore minerals in hinge zones of folds. Borehole NS0168. (D) Alternation of dark grey shale and layer parallel carbonate veins with chalcopyrite. The veins are folded and fractured with concentration of ore minerals in hinge zones of folds. Borehole NS0168. (E) Dark grey shale with layer parallel carbonate veins with pyrite and chalcopyrite, crosscut by cm-thick irregular veins consisting of calcite, quartz, pyrite and chalcopyrite. Borehole NS0168. (F) Massive vein consisting of calcite, quartz, massive chalcopyrite, bornite and carrollite and some feldspar and chlorite. Borehole CE570.

behaviour is observed between the two assemblages. The inclusions are completely frozen at −77 °C. In three inclusions, a solid phase formed around the vapor bubble during cooling at −40 °C, indicating the formation of clathrate. First melting of ice occurs from −32 °C and final melting of ice occurs mainly between −25.2 and −14.0 °C (Fig. 11). Three inclusions, which show the dissociation of clathrate around 5.4 °C, have Tm ice values between −6.3 and −4.0 °C. No second liquid phase, however, is present. Homogenization of the fluid inclusions into the liquid occurs between 80 and 172 °C (Fig. 12).

5.2. Interpretation

The first melting temperatures are clearly observed in all generations from −32 °C onwards and mostly below −22.9 °C (the eutectic temperature of the H_2O–NaCl–KCl system). This suggests a H_2O–NaCl/KCl–$MgCl_2$ composition of the fluid inclusions (Roedder, 1984; Shepherd et al., 1985). The formation of clathrates in a few inclusions in the layer parallel and massive veins without the formation of a second liquid phase indicates the presence of a minor amount of a gaseous component in these inclusions. With the FLINCOR program of Brown (1989) and the equation of state of Brown and Lamb (1989), the final melting temperatures are used to calculate the salinity of the fluid in the binary H_2O–NaCl system and are therefore expressed as equivalent wt.% NaCl. Fluid inclusions that show clathrate melting are not used in the calculations. The salinity of the inclusions with an unknown origin in the layer parallel veins ranges between 10.2 and 19.8 eq. wt.% NaCl. The salinity of the secondary inclusions in this vein generation clusters between 18.1 and 18.6 eq. wt.% NaCl. In the irregular veins, salinity ranges between 21.1 and >23.2 eq. wt.% NaCl and in the massive veins between 17.8 and >23.2 eq. wt.% NaCl. The values higher than

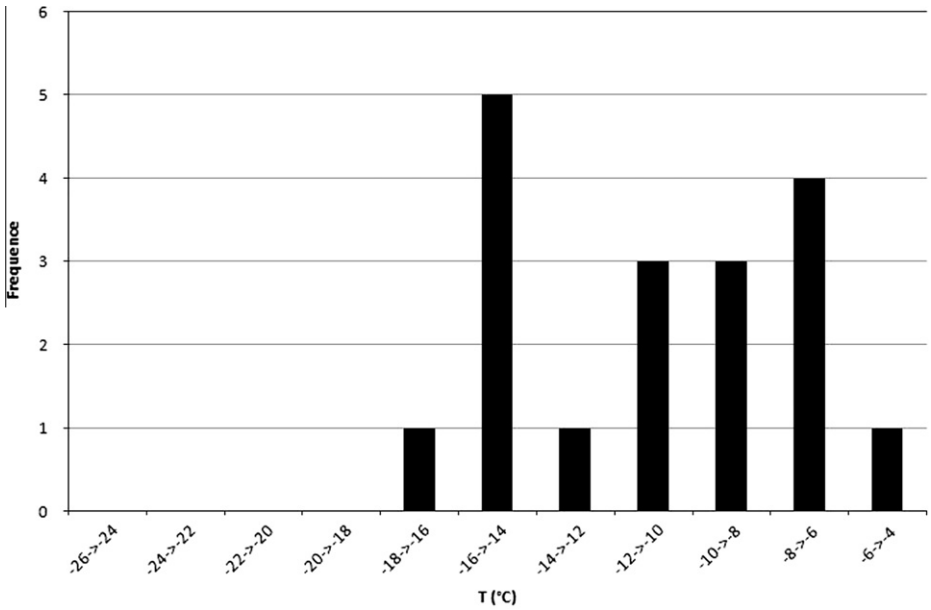

Fig. 7. Final melting temperature of ice of fluid inclusions in quartz from layer parallel veins at Nkana.

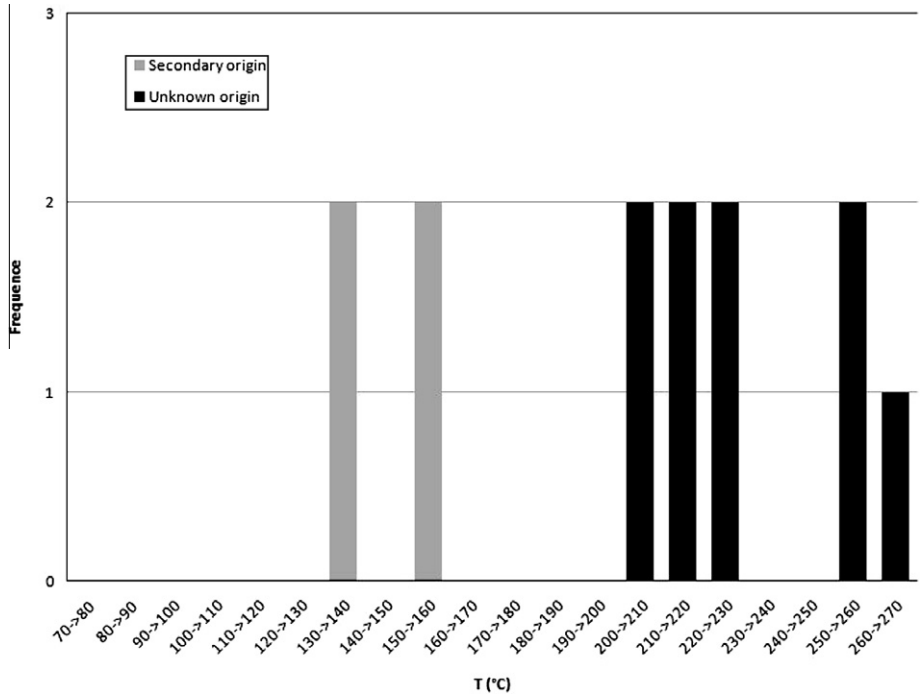

Fig. 8. Homogenization temperature of fluid inclusions in quartz from layer parallel veins at Nkana.

23.2 eq. wt.% NaCl are due to Tm ice values below −21.2 °C (cf. Bodnar, 1993).

5.3. Discussion

5.3.1. Orogenic fluids

The fluid inclusions with an unknown origin in the layer parallel veins have higher homogenization temperatures than the secondary fluid inclusions in this vein generation and the fluid inclusions in the other vein generations. The maximum range of the isochores of these fluid inclusions is given in Fig. 13. If a lithostatic pressure of the fluid is assumed, based on the origin of the layer parallel veins, the isochores starting at the highest Th value cross the lithostatic gradient of 50 °C/250 bars around 2100 bar and 450 °C, which is the temperature of metamorphism proposed for this area. The lithostatic pressure of 2100 bars corresponds to a burial depth of 8.4 km. The fluid inclusions could represent primary inclusions or secondary inclusions that were trapped during the main period of metamorphism between 592 and 520 Ma (Rainaud et al., 2005; John et al., 2004). Lower geothermal gradients result in unrealistically high pressures and temperatures. Hydrothermal fluid pressure gradients of 30–50 °C/100 bar result in a trapping temperature around 300 °C and a pressure of 750 bars (7.5 km). Since the layer parallel veins are interpreted to have formed at

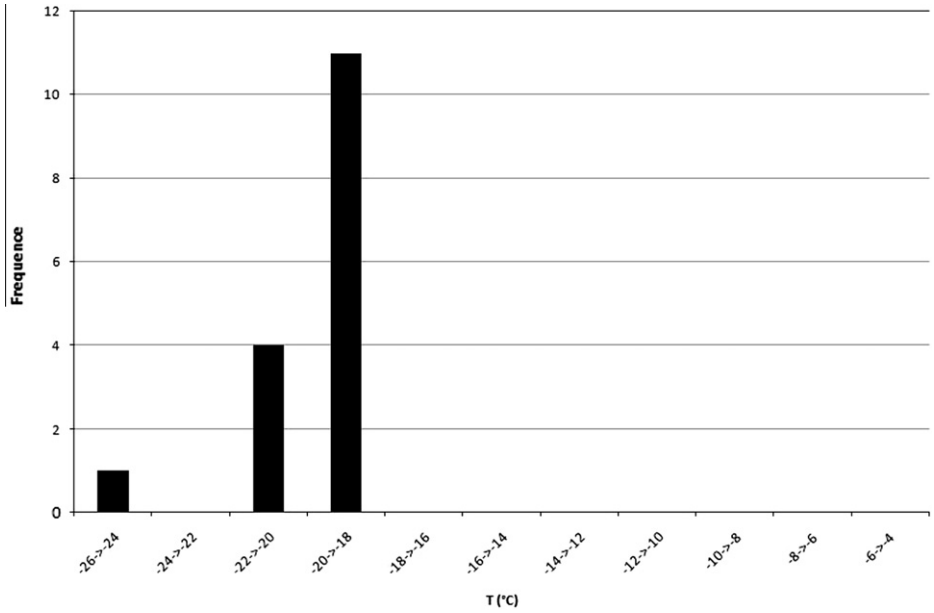

Fig. 9. Final melting temperature of ice of two fluid inclusions in quartz from irregular veins at Nkana.

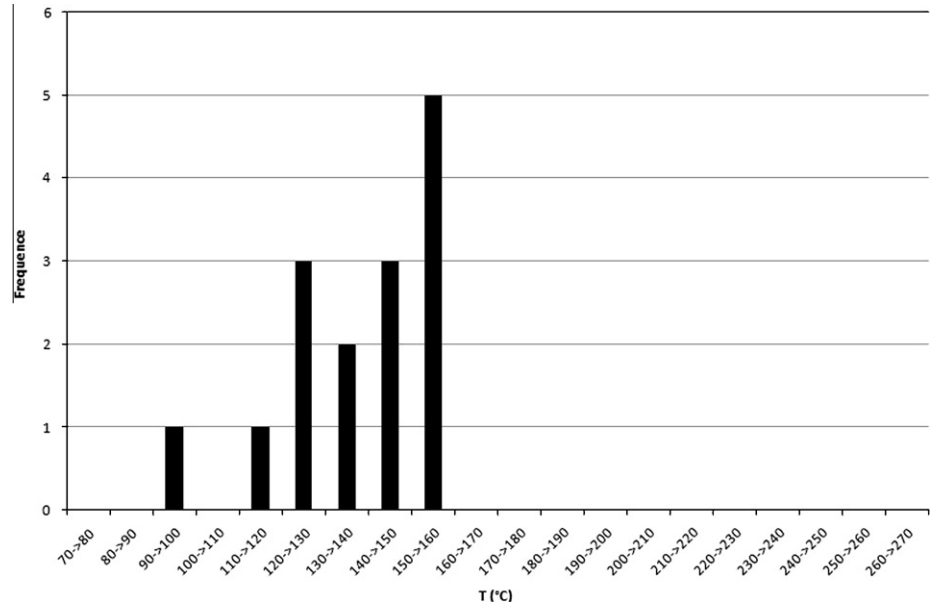

Fig. 10. Homogenization temperature of fluid inclusions in quartz from irregular veins at Nkana.

lithostatic pressure at maximum burial, this temperature and pressure would imply trapping as secondary fluid inclusions after peak metamorphism at ~530 Ma, during retrograde metamorphism.

Greyling (2009) studied early and late orogenic fluids at Chambishi, Nchanga and Nkana. The fluids present in bedding parallel veins are classified as early orogenic veins. Based on laser ablation inductively coupled plasma mass spectrometry (LA-ICPMS) analysis of individual inclusions, the early orogenic fluids at Nkana have a H_2O–NaCl–KCl–$MgCl_2$ composition with possibly $CaCl_2$ (Greyling, 2009). Calcium has not been analyzed by Greyling (2009). Raman analysis also indicated the presence of CO_2 and CH_4 in some inclusions (Greyling, 2009). The vapor phase analyzed contains 84 mol% CH_4 and 16 mol% CO_2. The composition of the inclusions is similar to that proposed for the fluid inclusions in the layer parallel veins based on microthermometry. Greyling (2009) proposed the early orogenic fluid inclusions were trapped near hydrostatic conditions at a maximum temperature and pressure of 260 °C and 800 bar, which corresponds to a depth of 8 km at a hydrothermal gradient of 30 °C/100 bar. A similar temperature and pressure was proposed by Greyling et al. (2005) for early orogenic fluids at Chambishi, based on the crossing of the isochores of low saline aqueous inclusions with the isochore of CH_4 in fluid inclusion planes. However, the co-genetic relationship between these fluid inclusion planes and the exact timing is not demonstrated. If the inclusions formed during formation of the layer parallel veins, a lithostatic pressure is more likely than a hydrostatic one. In addition, the precipitation of biotite in these veins favours a precipitation temperature higher than 260 °C (Philpotts and Ague, 2009).

5.3.2. Late- to post-orogenic fluids

The secondary fluid inclusions in layer parallel veins have a high salinity and Th range comparable to the fluid inclusions of

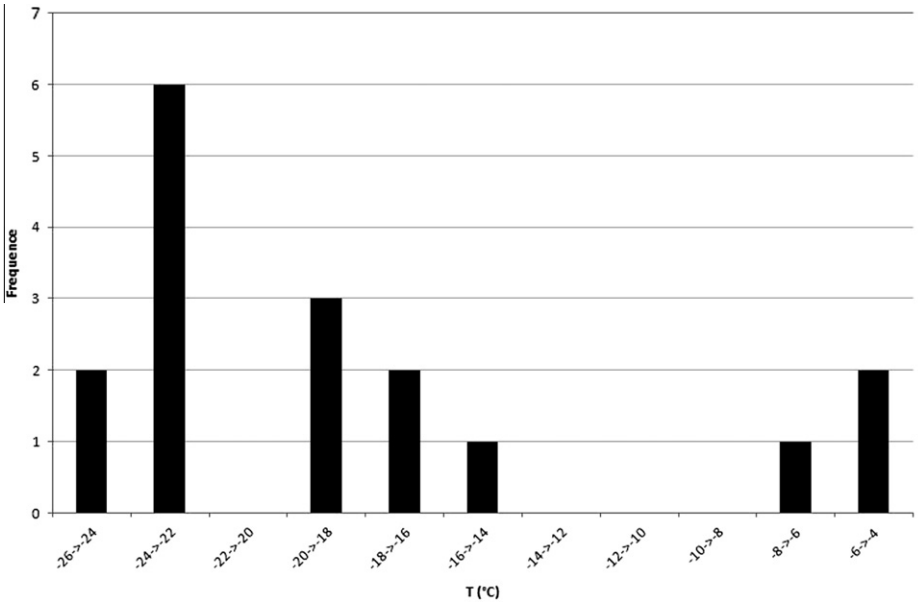

Fig. 11. Final melting temperature of ice of fluid inclusions in quartz from massive veins at Nkana.

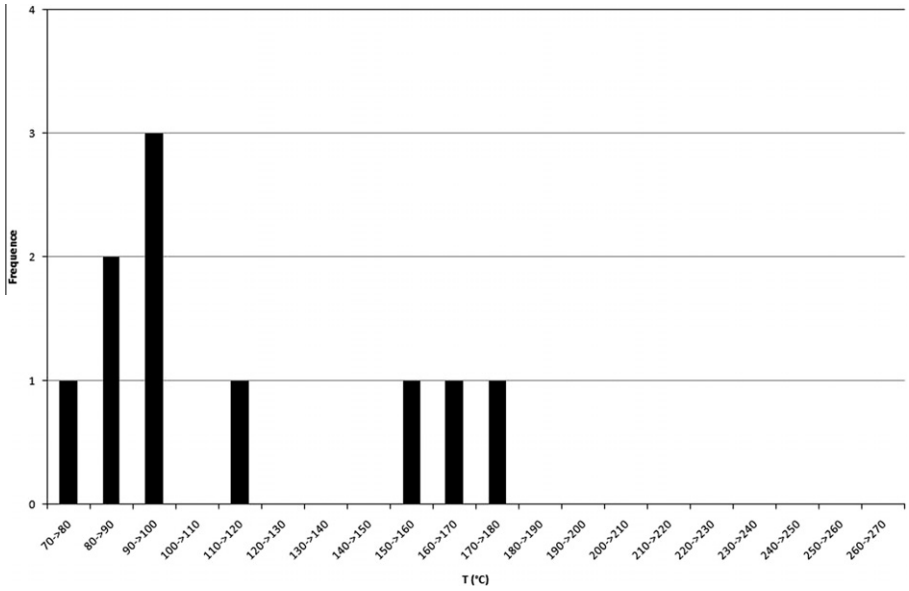

Fig. 12. Homogenization temperature of two fluid inclusions in quartz from massive veins at Nkana.

unknown origin in the irregular veins and the secondary fluid inclusions in the massive veins. The possible range of trapping temperatures, indicated by the crossing of the isochores with the different fluid pressure gradients, lies between 100 and maximum 250 °C (Fig. 13). This is much lower than the metamorphic temperatures recorded in the area and indicated by the mineral assemblages in the veins. These fluid inclusions were clearly enclosed after precipitation of the different vein generations and possibly during retrograde metamorphism. Two retrograde pathways can be proposed during cooling and exhumation of the rocks at Nkana (Fig. 13). The first path (1) is characterized by a decrease in temperature, representing the re-equilibration of the geothermal gradient, which outpaces the pressure decrease and represents exhumation. In the second path (2), exhumation causes an important change in pressure and a slower decrease in temperature. John et al. (2004) reported an evolution similar to retrograde path 2 in the Solwezi Dome situated at ~200 km to the west of Nkana in the Domes region. However, reported peak metamorphism was much higher than at Nkana and reached whiteschist facies.

Secondary inclusions in late orogenic veins have been studied by Greyling (2009). At Nkana, the temperatures of first melting lie between −50 and −21 °C, with most values below −35 °C. A H_2O–NaCl–KCl–$MgCl_2$ composition with a more pronounced amount of $CaCl_2$ in some inclusions can be proposed. Homogenization temperatures range between 98 and 400 °C, with a peak in the distribution around 150 °C and salinities between 5 and 21.6 eq. wt.% NaCl. The secondary fluid inclusions studied in the three vein generations have a similar composition, but salinities are mostly higher, and Th values fall within the lower range of the values reported by Greyling (2009). Clara et al. (2009) analyzed secondary inclusions in quartz from late massive veins at Mindola. The inclusions have a H_2O–NaCl–$CaCl_2$-X composition, with X the presence

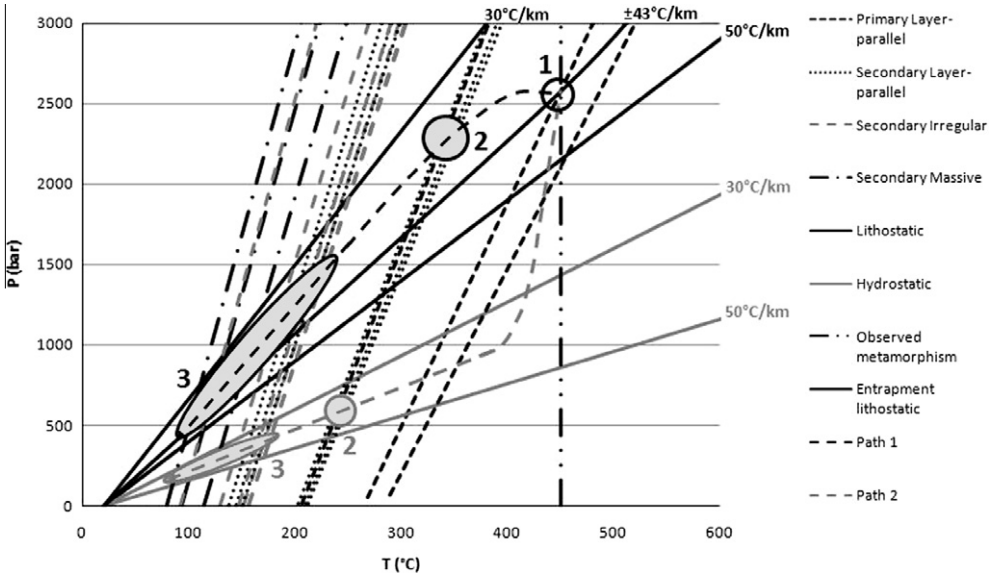

Fig. 13. Pressure–temperature plot with the isochores of the fluid inclusions from the three vein generations studied at Nkana. Lithostatic and hydrostatic fluid pressures are indicated. The dotted vertical line represents the maximum temperature reached at Nkana based on the observed metamorphism. The dashed lines indicate two possible retrograde paths, starting from the assumed entrapment P-T of the high temperature fluid inclusion assemblage in the layer parallel veins.

of a gaseous component in some inclusions as indicated by the melting of clathrates between −4.7 and 3 °C. The salinity of the inclusions without any evidence for this gaseous component varies between 15.97 and 23.00 wt.% based on the melting of hydrohalite and the final melting of ice. Homogenization temperatures are low and lie between 74 and 121 °C. The calcium content seems to vary within the Nkana–Mindola area, as has been reported for the Chambishi deposit by Greyling (2009). Dolomitization and albitization of Ca-rich feldspars are common processes in sedimentary basins, which cause the enrichment of brines in calcium (Carpenter et al., 1976; Heijlen et al., 2001). Both are important alteration processes in the Zambian Copperbelt (Selley et al., 2005). The reason for the local or temporal variation of the calcium content is unclear, however, it postdates the late mineralization phase at 525.7 Ma characterized by the presence of molybdenite and anhydrite.

6. Stable isotopic composition

6.1. Oxygen and carbon

The carbon and oxygen isotopic composition of the carbonates in the veins has been determined at the University of Erlangen-Nürnberg (Germany). Sample powders were selectively drilled from the nodules and the different vein generations at Leuven. The powders reacted with 100% phosphoric acid with a density >1.9 at 75 °C (cf. Wachter and Hayes, 1985). Oxygen isotopic compositions of dolomite were corrected for fractionation effects resulting from the reaction with the hot acid, using the fractionation factors given by Rosenbaum and Sheppard (1986). The analyses were performed on a Kiel III carbonate preparation line connected online to a ThermoFinnigan 252 Mass spectrometer. All values are reported in per mil relative to the belemnite standard of the Cretaceous Peedee Formation (‰ V-PDB). Reproducibility was checked by replicate analysis of laboratory standards and is better than ±0.03‰ for $\delta^{13}C$ and ±0.05‰ for $\delta^{18}O$ at the 1σ level.

No systematic difference is observed between the dolomite and calcite from the same generation in the Ore Shale (Fig. 14). Two ranges can be observed in the data. A first range is characterized by a rather small spread in $\delta^{18}O$ values around −15.5‰ V-PDB and a large variation in $\delta^{13}C$ values between −25‰ and −12‰

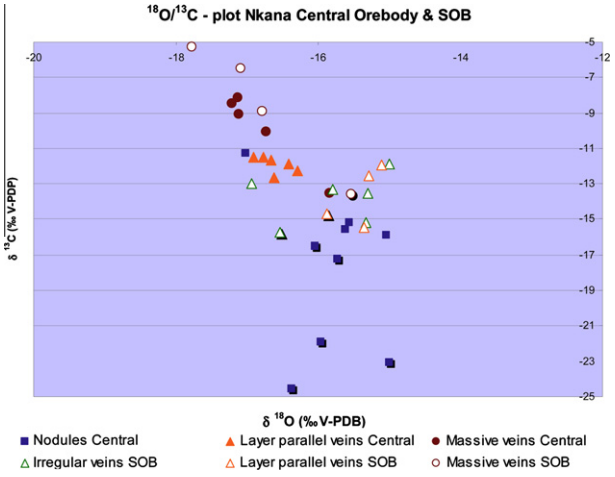

Fig. 14. Oxygen and carbon isotope data from calcite and dolomite in nodules and veins from Nkana Central and South Orebodies. Data points from dolomites are shaded with black, while calcite samples are not.

V-PDB. This variation in $\delta^{13}C$ values is mainly expressed in the carbonate nodules. The second range shows an increase in the carbon isotopic composition and a decrease in the oxygen isotope values of the carbonates from the layer parallel veins, especially from Central Orebody at Nkana, to the massive veins.

All observed isotope signatures are more negative than the values of Late Neoproterozoic marine carbonates, which range between −4.0‰ and 4.0‰ for $\delta^{13}C$ and between −8.0‰ and −4.0‰ for $\delta^{18}O$ (Veizer and Hoefs, 1976; Lindsay et al., 2005). The first range has been observed in several isotopic studies of the carbonates associated with Cu–Co mineralization in the Copperbelt (Sweeney et al., 1986; Annels, 1989; Sweeney and Binda, 1989). Selley et al. (2005) examined the different possible explanations for this range and concluded that negative shifts up to 30‰ in $\delta^{13}C$ (from +5‰ to −25‰ V-PDB in their dataset of 369 isotope analyses) are related to oxidation of organic matter or methane with the formation of CO_2 or HCO_3^-.(cf. Irwin et al., 1977; Muchez et al., 1998). The $\delta^{18}O$ values lower than Neoproterozoic marine

carbonates can be explained by a fluid with a $\delta^{18}O$ value lower than the seawater composition or by a higher precipitation temperature. Taking into account the high precipitation temperatures of the carbonates as indicated by the numerous fluid inclusion studies in the Zambian Copperbelt (e.g. Greyling, 2009), this is the most straightforward explanation for the $\delta^{18}O$ values of the dolomites in the veins (Annels, 1989; Muchez et al., 2008). The calculation of the range in oxygen isotopic composition of the ambient fluid from which dolomite with a $\delta^{18}O$ value of −15‰ V-PDB precipitated between 250 °C and 400 °C, leads to values between +5.6 and +10.3 V-SMOW, using the empirical fractionation equation for dolomite of Northrop and Clayton (1966). This range is much higher than the oxygen isotopic composition of meteoric and sea water.

The second range shows an increase in $\delta^{13}C$ values in the majority of the late massive veins. Such an increase can be explained by ongoing oxidation in the system with a relative depletion in ^{12}C in the remaining organic carbon. A contribution of ^{13}C enriched HCO_3^- from the dissolution of Neoproterozoic carbonates, such as present in the barren gap between Nkana and Mindola, can not be excluded (cf. Jordaan, 1961). However, this is not reflected in a common increase in the carbon and oxygen isotopic composition as should be expected. The decrease in the $\delta^{18}O$ values in the massive veins can be due to an increase of the precipitation temperature of the massive veins compared to the other veins, to a decrease of the $\delta^{18}O$ of the mineralizing fluid or a combination of both. The maximum difference in the oxygen isotope values between the massive and the irregular or layer parallel veins is 3‰, i.e. between −18‰ and −15‰ V-PDB (Fig. 14). Taking into account a temperature of 400 °C for the layer parallel veins and a constant $\delta^{18}O$ value of the ambient water, a shift of 3‰ V-PDB corresponds to an increase in precipitation temperature of >200 °C in the massive veins, using the empirical fractionation equation for dolomite of Northrop and Clayton (1966). This value is not realistic and the decrease in $\delta^{18}O$ of the dolomites can not only be explained by an increase in temperature. If the variation is only due to a difference in the isotopic composition of the ambient fluid, then the calculation of the oxygen isotopic composition of this fluid at 400 °C, precipitating dolomites with a $\delta^{18}O$ value of −18‰ and −15‰ V-PDB, reveals an isotopic composition of +7.2‰ V-SMOW and +10.3‰ V-SMOW respectively. The latter two values lie in the field of metamorphic waters (Sheppard, 1986) and such a variation in oxygen isotopic composition is common in metamorphic settings (Gray et al., 1991; Marquer and Burkhard, 1992; Dewaele et al., 2004). Variations are due to different source rocks of the fluids, migration pathways, varying water–rock ratios and the scale of buffering by the rocks (Knoop et al., 2002; Kenis et al., 2005; Berwouts et al., 2008).

This study confirms recent stable isotope research from the Copperbelt, which demonstrates that it is essential to differentiate the Cu–Co mineralization phases and to analyze them separately (Muchez et al., 2008; El Desouky et al., 2009a, accepted for publication).

6.2. Sulphur

The sulphur isotopic composition of the samples was analyzed by in situ laser combustion from standard polished sections. An area of 300–400 μm diameter of the sulphide minerals were combusted using a Spectron Lasers 902Q CW Nd:YAG laser, in the presence of excess oxygen (Fallick et al., 1992). The released CO_2 gas was purified in a vacuum line, which operates similar to a conventional sulphur extraction line (Kelley and Fallick, 1990). The sulphur isotopic composition of the purified SO_2 gas was measured using a VG SIRA II gas mass spectrometer. Sulphur isotope compositions are reported in standard per mil (‰) relative to the Canyon Diablo Troilite (V-CDT). The analytical precision, based on replicate measurements of international standards NBS-123 and IAEA-S-3 as well as internal lab standard CP-1 (Scottish Universities Environmental Research Centre), was ±0.2‰.

Taking into account the position of the sulphides analyzed in the paragenetic sequence (Fig. 15), an increase in the $\delta^{34}S$ values can be recognized from the early pyrite ($\delta^{34}S$ between −16.0‰ and −9.7‰ V-CDT in disseminated sulphides and lenses), to sulphides in the layer parallel and irregular veins ($\delta^{34}S$ between −9.2‰ and −2.0‰ V-CDT) and finally sulphides in the massive veins (1.3–2.0‰ V-CDT). The $\delta^{34}S$ values of the nodules vary between −7.0‰ and 1.0‰ V-CDT. Four of the five values correspond to sulphides from the layer parallel and irregular veins. The framboidal and massive pyrites have distinctly negative $\delta^{34}S$ values, comparable to black shale-hosted diagenetic pyrite at Nchanga (McGowan et al., 2003, 2006). Assuming a marine sulphate source with a signature of Late Neoproterozoic seawater (17.5‰ V-CDT, Claypool et al., 1980), the fractionation for the early sulphides ranges between 27.2‰ and 33.5‰. Such fractionation is characteristic for bacterial sulphate reduction (BSR; Machel et al., 1995). With time, the sulphides became enriched in heavier S. This is interpreted as the result of the mixing of S, remobilized from early sulphides with a low $\delta^{34}S$ value, with S derived from thermochemical reduction of sulphate. Anhydrite was very abundant during metamorphism as indicated by their omnipresence in massive veins and as a widespread alteration phase (Selley et al., 2005; Brems et al., 2009). With time, the sulphur derived from TSR became more important relative to sulphur derived from BSR. The $\delta^{34}S$ value of the anhydrite present in the massive veins varies around 17.5‰ (Fig. 15), which corresponds to the average value reported by Claypool et al. (1980) for the sulphur isotopic composition of Neoproterozoic seawater. McGowan et al. (2006) reported $\delta^{34}S$ values of −1‰ to 12‰ V-CDT for the sulphides from the Lower Orebody at Nchanga (Zambian Copperbelt) and of 5–12‰ V-CDT for the Upper Orebody. They interpreted the latter values as characteristic for thermochemical reduction of sulphate enriched hydrothermal fluid at the site of mineralization, without any evidence for a contribution of bacteriogenic sulphide. This interpretation is in agreement with the model proposed.

7. Strontium isotopic composition

For the determination of Rb and Sr concentrations and $^{87}Sr/^{86}Sr$ isotope ratios, approximately 50 mg of carbonate powder, drilled from the veins, was weighed into a screw-capped Savillex® PFA vial and dissolved in 1 mL of 6 M HCl on a hotplate at 120 °C. The digests were subsequently evaporated to dryness and taken up in 7 M HNO_3. Rb and Sr concentrations were determined using a PerkinElmer SCIEX Elan 5000 quadrupole-based ICP-MS instrument via standard addition. For isotope ratio analysis, strontium was isolated from the concomitant sample matrix using an extraction chromatographic resin (Sr spec™, Horwitz et al., 1991) following a procedure that was described in detail by De Muynck et al. (2009). After loading the sample in 7 M HNO_3 onto the resin, matrix elements were quantitatively removed by rinsing the resin with 7 M HNO_3 and the purified Sr fraction was recovered by rinsing the resin with 0.05 M HNO_3. $^{87}Sr/^{86}Sr$ ratios were determined using a Thermo Electron Neptune MC-ICP-MS instrument and normalized to the invariant $^{86}Sr/^{88}Sr$ ratio (=0.1194). More details concerning the measurement protocol followed can be found in De Muynck et al. (2009). Repeated analyses ($n = 14$) of NIST SRM 987 $SrCO_3$ over the duration of this study yielded a $^{87}Sr/^{86}Sr$ ratio of 0.710259 ± 0.000029 (2s), in excellent agreement with the accepted $^{87}Sr/^{86}Sr$ ratio of this reference material (=0.710248, Thirlwall, 1991).

The strontium isotopic composition of the carbonates in the nodules and different vein generations show a wide range with

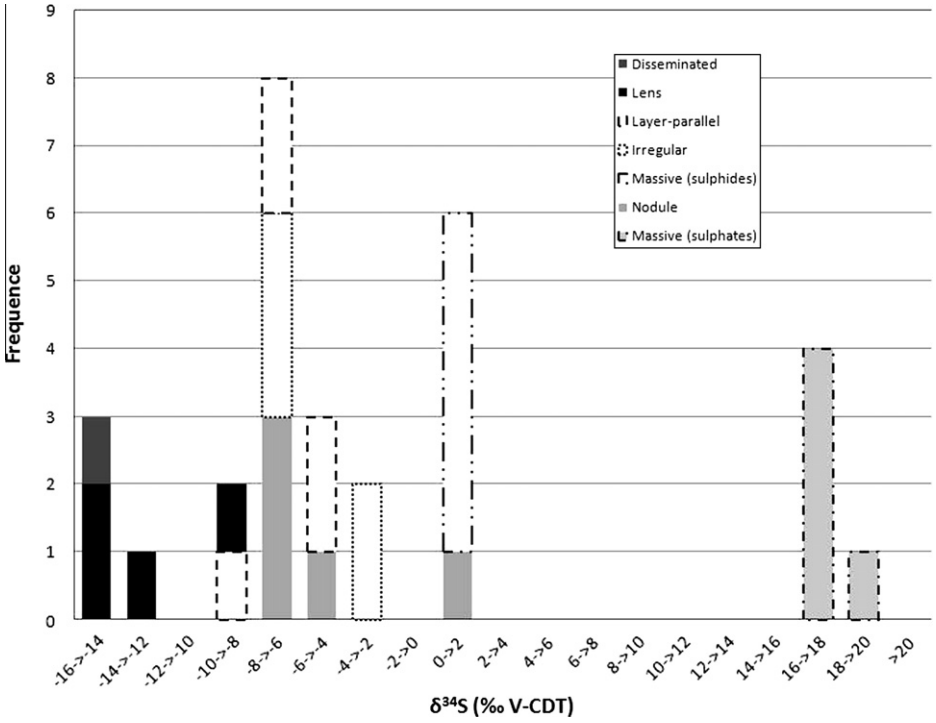

Fig. 15. Histogram of $\delta^{34}S$ values of sulphides in nodules and veins from Nkana.

$^{87}Sr/^{86}Sr$ values up to 0.75407 (Table 1). All values are significantly more radiogenic than the strontium isotopic composition of Neoproterozoic marine carbonates, which range between 0.7056 and 0.7087 (Jacobsen and Kaufman, 1999). Rb contents are low, especially when compared to the Sr content, except for one nodule sample and most layer parallel veins. The high Rb content in one nodule and four layer parallel veins is most likely due to the presence of small fyllosilicates at their margin (Table 1). To determine "initial" Sr isotopic compositions for these samples, corrections were performed using an age of 583 Ma. These corrections had a significant effect (Fig. 16). Because of their low Rb contents, this effect is insignificant for the other nodules and veins. For the massive veins an age of 525 has been used for the corrections. After this correction, the layer parallel veins are still more radiogenic than the nodules and the other veins (Fig. 17). A comparison with the scarce Rb–Sr data of the Neoproterozoic rocks and the basement shows that the veins are more radiogenic than the Roan carbonates analyzed by El Desouky et al. (2009b, accepted for publication) and the Kundelungu sandy dolomites (Haest et al., 2009) in the Congolese Copperbelt, but show a similar range as the granitic basement exposed in the Luina and Lubembe Domes (Ngoyi et al., 1991). However, the arkoses at Nchanga (Zambian Copperbelt) are also radiogenic with values equal and higher than 0.79364 (0.79275 at 880 Ma; Roberts et al., 2009). At this stage of research, this indicates interaction of the fluid precipitating the vein cements with the basement or sediments derived from it.

Table 1
Rb-Sr isotopic and concentration data for the carbonates in nodules and veins from Nkana. The asterisk indicates the likely presence of fyllosilicates in the samples analyzed since they occur at the margin of the nodule and the veins. The $^{87}Sr/^{86}Sr$ ratio has been recalculated to the estimated age of carbonate precipitation, i.e. 583 Ma for the nodules, layer parallel and irregular veins and 525 Ma for the massive veins.

Sample	Feature	1000/Sr ppm^{-1}	$^{87}Rb/^{86}Sr$ estimated	$^{87}Sr/^{86}Sr$ measured	$^{87}Sr/^{86}Sr$ 583 Ma	$^{87}Sr/^{86}Sr$ 525.7 Ma
CS08AC02	Massive vein	2.455	0.011	0.72546	–	0.72538
CE08AC14	Massive vein	1.632	0.001	0.72016	–	0.72015
CE08AC10	Massive vein	1.356	0.002	0.71928	–	0.71927
CE08AC42	Massive vein	2.203	0.002	0.72107	–	0.72106
NS06DB08	Massive vein	1.776	0.001	0.72935	–	0.72934
NS06DB19	Irregular vein	4.379	0.023	0.72722	0.72703	–
NS06DB01	Layer parallel vein*	3.953	0.088	0.73629	0.73556	–
NS06DB45	Irregular vein	4.880	0.033	0.72577	0.72550	–
NS06DB15	Layer parallel vein	5.373	0.035	0.73863	0.73834	–
NS08LL07	Layer parallel vein	7.634	0.028	0.74107	0.74084	–
NS06DB14	Layer parallel vein*	7.508	1.039	0.74431	0.73571	–
NS06DB01	Layer parallel vein*	24.710	2.395	0.75407	0.73424	–
CE08AC20	Layer parallel vein*	5.084	0.715	0.72924	0.72331	–
CE08AC12	Nodules	4.679	0.038	0.71797	0.71765	–
CE08AC02	Nodules	4.034	0.044	0.72689	0.72653	–
CE08AC34	Nodules	7.132	0.079	0.71672	0.71606	–
CE08AC03	Nodules	4.947	0.024	0.71892	0.71872	–
CE08AC05	Nodules*	7.409	0.316	0.72611	0.72349	–
NS06DB44	Irregular vein	5.669	0.046	0.72563	0.72524	–

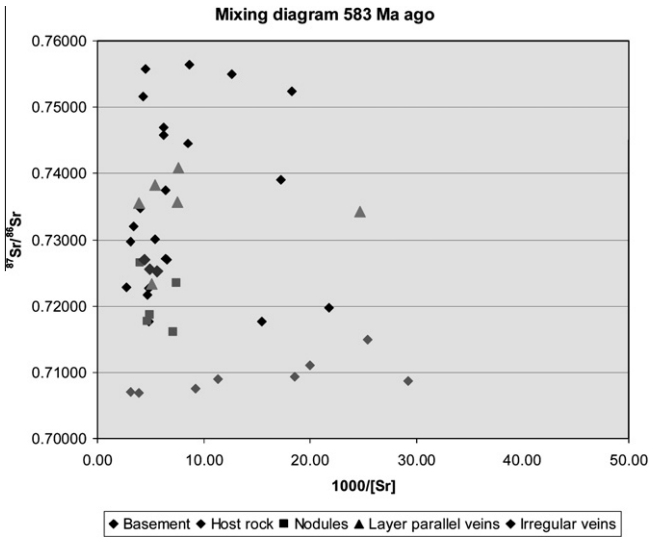

Fig. 16. Plot of the $^{87}Sr/^{86}Sr$ ratio versus 1000/Sr content of carbonates from nodules and veins from Nkana. The data from Katanga Supergroup rocks and from the basement are from Cahen et al. (1970a,b), Ngoyi et al. (1991), El Desouky et al. (accepted for publication) and Haest et al. (2009). All data are recalculated at an age of 583 Ma, based on the age proposed by Barra et al. (2004) for the vein-type sulphides.

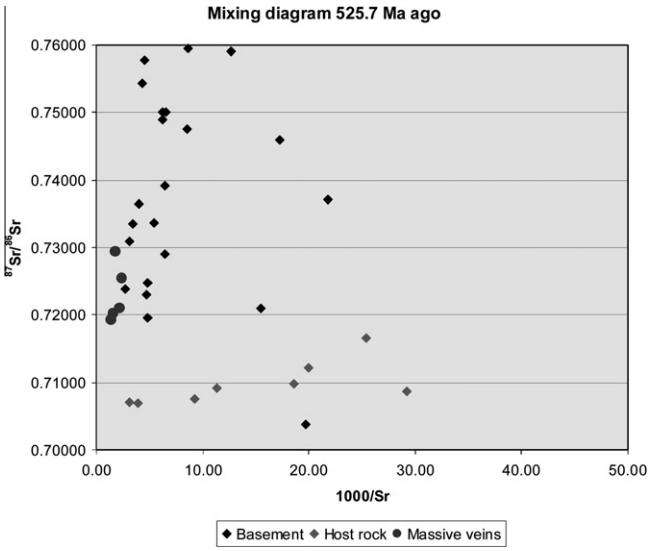

Fig. 17. Plot of the $^{87}Sr/^{86}Sr$ ratio versus 1000/Sr content of carbonates from massive veins at Nkana. The data from Katanga Supergroup rocks and from the basement are from Cahen et al. (1970a,b), Ngoyi et al. (1991), El Desouky et al. (accepted for publication) and Haest et al. (2009). All data are recalculated at an age of 525 Ma, based on the age proposed by Barra et al. (2004) for the massive veins with chalcopyrite and molybdenite.

8. Conclusion

This geochemical and microthermometric study has demonstrated an evolution in geochemical characteristics of the successive mineralization/remobilization at Nkana, which can be related to the geodynamic evolution (Fig. 18). During initial rifting (Fig. 18A), pyrite precipitated due to bacterial sulphate reduction as indicated by distinctly negative $\delta^{34}S$ values. The replacement of this pyrite by Cu-sulphides could have occurred at any subsequent stage. Pseudomorphosed anhydrite nodules are filled with

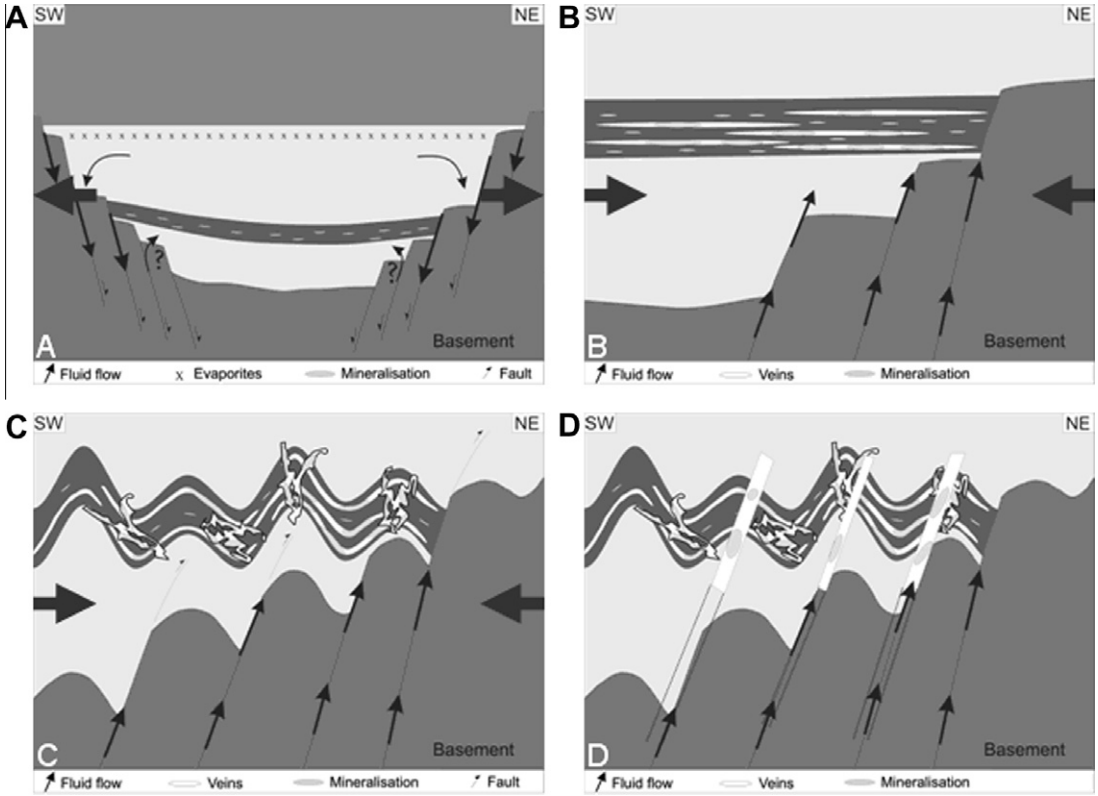

Fig. 18. Metallogenic model for Nkana Cu–Co ore deposit. (A) Initial rifting and precipitation of early diagenetic pyrite and possibly Cu–Co sulphides. (B) Start of basin inversion and mineralization in layer parallel veins. (C) Folding and remobilization/mineralization of sulphides in fold hinges and irregular veins. (D) Post-folding development of massive, often intensely mineralized veins.

quartz, carbonates, biotite, muscovite and sulphides, which have a metamorphic origin. $\delta^{13}C$ values of the carbonates range between $-15‰$ and $-25‰$ V-PDB in the nodules. This range is explained by the oxidation of organic matter or methane.

Layer parallel veins formed at supralithostatic pressures during the initial phase of basin inversion (Fig. 18B). During further compression, the rocks and the layer parallel veins were folded, with a concentration of minerals in the hinge zones of the folds (Fig. 18C). Highly irregular veins likely formed at high fluid pressures during the main phase of orogenesis. Unfolded massive veins crosscut all preceding phases (Fig. 18D). The presence of some new mineral phases like molybdenite and anhydrite suggests that a different fluid was responsible for the mineralization of these veins. The presence of carrolite and cobalt-bearing calcite are indicative of a higher Co content in this late vein generation. The evolution to more negative $\delta^{18}O$ values from the layer parallel veins and the irregular veins towards the massive veins can partly be due to a higher precipitation temperature of the massive veins, but mainly reflects a change of the oxygen isotopic composition of the metamorphic water. The decrease in the $\delta^{18}O$ values is associated with an increase in the $\delta^{13}C$ values, which is explained by an ongoing oxidation of in situ organic mater in a relatively closed system. An increase in $\delta^{34}S$ values is recognized from the pyrites, to sulphides in the layer parallel and irregular veins and finally in the massive veins. Apparently the sulphides became enriched in heavier S as a result of the mixing of S remobilized from early sulphides, with S derived from thermochemical reduction of sulphate. With time the sulphur derived from TSR became more important. Preliminary Sr isotopic data indicate there was interaction between the basement or sediments derived from it and the fluid which was responsible for the precipitation of the different vein generations.

All the measured fluid inclusions in the different vein generations have a dominant H_2O–NaCl/KCl–$MgCl_2$ composition. The formation of clathrates in a few inclusions in the layer parallel and massive veins indicates the presence of a minor amount of a gaseous component. The fluid inclusions with an unknown origin in the layer parallel veins have higher homogenization temperatures than the secondary fluid inclusions in this vein generation and the fluid inclusions in the other vein generations. These inclusions could be primary inclusions or secondary inclusions that were trapped during the main phase of metamorphism. The secondary fluid inclusions in layer parallel veins have a similar high salinity and homogenization temperature range as the fluid inclusions of unknown origin in the irregular veins and the secondary fluid inclusions in the massive veins. The possible range of trapping temperatures is between 100 and 250 °C. These fluid inclusions were trapped after formation of the different vein generations and possibly during retrograde metamorphism. These inclusions are not representative of the fluids which led to the precipitation of the veins.

Acknowledgements

We are grateful to the geologists of Mopani Copper Mines Plc and especially to Stanley Shasauka, Whiteson Silondwa and Alex Simutowe for assisting us with the underground mapping, providing the borehole data and the many stimulating discussions. We largely appreciate the constructive comments by two anonymous reviewers. We thank Herman Nijs for the careful preparation of the numerous thin and polished sections and the doubly polished wafers. We also thank Dr. M. Joachimski for measuring the oxygen and carbon isotopic composition of the carbonates.

This research is financially supported by research Grants G.0585.06 and G.0414.08 of the FWO-Vlaanderen.

References

Annels, A.E., 1974. Some aspects of the stratiform ore deposits of the Zambian Copperbelt and their genetic significance. In: Batholomé, P. (Ed.), Gisements stratiformes et provinces cuprifères. Centenaire de la Société Géologique de Belgique, Liège, pp. 235–254.

Annels, A.E., 1989. Ore genesis in the Zambian Copperbelt with particular reference to the Northern Sector of the Chambishi Basin. In: Boyle, R.W., Brown, A.C., Jeferson, C.W., Jowett, E.C., Kirkham, R.V. (Eds.), Sediment-Hosted Stratiform Copper Deposits. Geological Association of Canada, Special Paper 36, pp. 427–452.

Annels, A.E., Simmonds, J.R., 1984. Cobalt in the Zambian Copperbelt. Precambrian Research 25, 75–98.

Armstrong, R.A., Master, S., Robb, L.J., 2005. Geochronology of the Nchanga Granite, and constraints on the maximum age of the Katanga supergroup, Zambian Copperbelt. Journal of African Earth Sciences 42, 32–40.

Bard, P.G., Jordaan, J., 1963. Some structural features associated with the Rokhana orebodies. In: Lombard, J., Nicolini, P. (Eds.), Stratiform Copper Deposits in Africa. 2nd Part: Tectonics. Association of African Geological Surveys, Paris, pp. 179–191.

Barra, F., Broughton, D., Ruiz, J., Hitzman, M., 2004. Multi-Stage Mineralization in the Zambian Copperbelt based on Re–Os Isotope Constraints. The Geological Society of America Abstracts with Program 36, Denver Annual Meeting, 7–10 November 2004.

Bartholomé, P., 1974. On the diagenetic formation of ores in sedimentary beds, with special reference to Kamoto, Shaba, Zaïre. In: Bartholomé, P., de Magnée, I., Evrard, P., Moreau, J. (Eds.), Gisements Stratiformes et Provinces Cuprifères. Société Géologique de Belgique, Liège, pp. 203–213.

Berwouts, I., Van Noorden, M., Muchez, Ph., Boyce, A.J., Sintubin, M., 2008. Inferring intermediate-scale fluid flow in a heterogeneous metasedimentary multilayer sequence during progressive deformation: evidence from the Monts d'Arrée slate belt (Brittany, France). Geofluids 8, 143–158.

Binda, P.L., Mulgrew, J.R., 1974. Stratigraphy of copper occurrences in the Zambian Copperbelt. In: Batholomé, P. (Ed.), Gisements stratiformes et provinces cuprifères. Centenaire de la Société Géologique de Belgique, Liège, pp. 215–233.

Bodnar, R.J., 1993. Revised equation and table for determining the freezing point depression of H_2O–NaCl solutions. Geochimica et Cosmochimica Acta 57, 683–684.

Brems, D., Muchez, Ph., Sikazwe, O., Mukumba, W., 2009. Metallogenesis of the Nkana copper–cobalt South Orebody, Zambia. Journal of African Earth Sciences 55, 185–196.

Brown, E.B., 1989. FLINCOR: a microcomputer program for the reduction and investigation of fluid inclusions data. American Mineralogist 74, 1390–1393.

Brown, E.B., Lamb, W.M., 1989. P-V-T properties of fluids in the system $H_2O \pm CO_2 \pm NaCl$: new graphical presentations and implications for fluid inclusion studies. Geochimica et Cosmochimica Acta 53, 1209–1221.

Cahen, L., Delhal, J., Deutsch, S., Grögler, N., Pasteels, P., 1970a. The age of the Roan Antelope and Mufulira granites (Copperbelt of Zambia). In: Cahen, L., Delhal, J., Deutsch, S., Grögler, N., Ledent, D., Pasteels, P. (Eds.), Three Contributions to the Geochronology and Petrogenesis of Granitic Rocks in the Copperbelt of Zambia and Southeast Katanga Province (Republic of the Congo). Koninklijk Museum voor Midden-Afrika, Tervuren, Belgium, Annalen Reeks 8, vol. 65, pp. 15–42.

Cahen, L., Delhal, J., Ledent, D., 1970b. On the age and petrogenesis of the microcline-bearing pegmatite veins at Roan Antelope and at Musoshi (Copperbelt of Zambia and S-E Katanga). In: Cahen, L., Delhal, J., Deutsch, S., Grögler, N., Ledent, D., Pasteels, P. (Eds.), Three Contributions to the Geochronology and Petrogenesis of Granitic Rocks in the Copperbelt of Zambia and Southeast Katanga province (Republic of the Congo). Koninklijk Museum voor Midden-Afrika, Tervuren, Belgium, Annalen Reeks 8, vol. 65, pp. 43–68.

Cailteux, J., 1994. Lithostratigraphy of the Neoproterozoic Shaba-type (Zaire) Roan supergroup and metallogenesis of associated stratiform mineralization. Journal of African Earth Sciences 19, 279–301.

Cailteux, J.L.H., Kampunzu, A.B., Lerouge, C., Kaputo, A.K., Milesi, J.P., 2005. Genesis of sediment-hosted stratiform copper–cobalt deposits, Central African Copperbelt. Journal of African Earth Sciences 42, 134–158.

Cailteux, J.L.H., Kampunzu, A.B., Lerouge, C., 2007. The Neoproterozoic Mwashya–Kansuki sedimentary succession in the Central African Copperbelt, its Cu–Co mineralization, and regional correlations. Gondwana Research 11, 414–431.

Carpenter, A.B., Trout, M.L., Pickett, E.E., 1976. Preliminary report on the origin and chemical evolution of lead- and zinc-rich oil field brines in central Mississippi. Economic Geology 69, 1191–1206.

Clara, E., 2009. Petrographic, Mineralogical and Geochemical Study of the Mindola Cu–Co ore Deposit, Zambia. Master Thesis in Geology, K.U. Leuven, Belgium, p. 101.

Claypool, G.E., Holser, W.T., Kaplan, I.R., Sakai, H., Zak, I., 1980. The age curves of sulphur and oxygen isotopes in marine sulphate and their mutual interpretation. Chemical Geology 28, 199–260.

Clemmey, H., 1974. Sedimentary geology of a Late Precambrian copper deposit at Kitwe, Zambia. In: Bartholomé, P. (Ed.), Gisements stratiformes et provinces cuprifères. Centenaire de la Société Géologique de Belgique, Liège, pp. 255–265.

Cobbold, P.R., Rodrigues, N., 2007. Seepage forces, important factors in the formation of horizontal hydraulic fractures and bedding-parallel fibrous veins ('beef' and 'cone-in-cone'). Geofluids 7, 313–322.

Croaker, M., Selley, D., McGoldrick, P., Mwale, G., 2003. Basin architecture and structural characteristics of the Neoproterozoic Lower Roan sequence at Nkana–Mindola Cu–Co deposit, SE Chambishi basin, Zambia. In: Cailteux, J.L.H. (Ed.), Conference and Field Workshop Lubumbashi 2003, Proterozoic Sediment-Hosted base Metal Deposits of Western Gondwana.

Daly, M.C., Chakroborty, S.K., Kasolo, P., Musiwa, M., Mumba, P., Naidu, B., Namateba, C., Ngambi, O., Coward, M.P., 1984. The Lufilian arc and Irumide belt of Zambia: results of a geotraverse across their intersection. Journal of African Earth Sciences 2, 311–316.

De Cleyn, A., 2009. Petrographic, Mineralogical and Geochemical Study of the Nkana Cu–Co Central Orebody, Zambia. Master Thesis in Geology, K.U. Leuven, Belgium, p. 117.

Dechow, E., Jensen, M.L., 1965. Sulphur isotopes of some Central African sulphide deposits. Economic Geology 60, 894–941.

De Muynck, D., Huelga-Suarez, G., Van Heghe, L., Degryse, P., Vanhaecke, F., 2009. Systematic evaluation of a strontium-specific extraction chromatographic resin for obtaining a purified Sr fraction with quantitative recovery from complex and Ca-rich matrices. Journal of Analytical Atomic Spectrometry 24, 1498–1510.

Dewaele, S., Muchez, Ph., Banks, D.A., 2004. Fluid evolution along multistage composite fault systems at the southern margin of the Lower Palaeozoic Anglo-Brabant fold belt, Belgium. Geofluids 4, 341–356.

Dewaele, S., Muchez, Ph., Vets, J., Fernandez-Alonzo, M., Tack, L., 2006. Multiphase origin of the stratiform Cu–Co ore deposits in the western part of the Lufilian fold-and-thrust belt, Katanga (Democratic Republic of Congo). Journal of African Earth Sciences 46, 455–469.

El Desouky, H.A., Muchez, Ph., Cailteux, J., 2009a. Two Cu–Co sulfide phases and contrasting fluid systems in the Katanga Copperbelt, Democratic Republic of Congo. Ore Geology Reviews 36, 315–332.

El Desouky, H., Muchez, Ph., Schneider, J., Cailteux, J., 2009b. Stable (C–O) and radiogenic (Sr) isotope geochemistry of the Luiswishi and Kamoto Cu–Co ore deposits, Katanga Copperbelt, Democratic Republic of Congo. In: Williams, P.J. et al. (Eds.), Smart Science for Exploration and Mining, 10th Biennial SGA Meeting. James Cook University, Townsville, Australia, pp. 435–437.

El Desouky, H.A., Muchez, Ph., Boyce, A.J., Schneider, J., Cailteux, J.L.H., Dewaele, S., von Quadt, A., accepted for publication. Genesis of sediment-hosted stratiform copper–cobalt mineralization at Luiswishi and Kamoto, Katanga Copperbelt (Democratic Republic of Congo). Mineralium Deposita.

Fallick, A., McConville, P., Boyce, A.J., Burgess, R., Kelley, S.P., 1992. Laser microprobe stable isotope measurements on geological materials: some experimental considerations (with special reference to δ^{34} S in sulphides). Chemical Geology 101, 53–61.

Fanning, C.M., Link, P.K., 2004. U–Pb SHRIMP ages of Neoproterozoic (Sturtian) glaciogenic Pocatello formation, Southeastern Idaho. Geology 32, 881–884.

Fleischer, V.D., Garlick, W.G., Haldane, R., 1976. Geology of the Zambian Copperbelt. In: Wolf, K.H. (Ed.), Handbook of Strata-bound and Stratiform Ore Deposits; II. Regional Studies and Specific Deposits, Cu, Zn, Pb and Ag Deposits, vol. 6. Elsevier, New York, pp. 23–352.

Garlick, W.G., 1961. The syngenetic theory. In: Mendelsohn, F. (Ed.), The Geology of the Northern Rhodesian Copperbelt. MacDonald, London, pp. 146–165.

Garlick, W.G., 1964. Criteria of recognition of syngenetic sedimentary mineral deposits and veins formed by their remobilization. In: General Proceedings of the Eighth Commonwealth Mining and Metallurgical Congress, vol. 6, pp. 1393–1418.

Garlick, W.G., Fleischer, V.D., 1972. Sedimentary environment of Zambian copper deposition. Geologie en Mijnbouw 51, 277–298.

Goldstein, R.H., Reynolds, T.J., 1994. Systematics of Fluid Inclusions in Diagenetic Minerals. Sepm Short Course, vol. 32, p. 199.

Gray, D.R., Gregory, R.T., Durney, D.W., 1991. Rock-buffered fluid rock interaction in deformed quartz-rich turbidite sequences, eastern Australia. Journal of Geophysical Research 96, 19681–19704.

Greyling, L.N., Robb, L.J., Master, S., Boiron, M.C., Yao, Y., 2005. The nature of early basinal fluids in the Zambian Copperbelt: a case study from the Chambishi deposit. Journal of African Earth Sciences 42, 159–172.

Greyling, L.N., 2009. Fluid Evolution and Characterisation of Mineralising Solutions in the Central African Copperbelt. PhD Thesis, University of the Witwatersrand, Johannesburg, South Africa.

Haest, M., Muchez, Ph., Dewaele, S., Boyce, A.J., von Quadt, A., Schneider, J., 2009. Petrographic, fluid inclusion and isotopic study of the Dikulushi Cu–Ag deposit, Katanga (D.R.C.): implications for exploration. Mineralium Deposita 44, 505–522.

Haynes, D.W., 1986. Stratiformes copper deposits hosted by low-energy sediments: I. Timing of sulfide precipitation – an hypothesis. Economic Geology 81, 250–265.

Heijlen, W., Muchez, Ph., banks, D.A., 2001. Origin and evolution of high-salinity, Zn–Pb mineralizing fluids in the Variscides of Belgium. Mineralium Deposita 36, 165–176.

Hoffman, P.F., Kaufman, A.J., Halverson, G.P., Schrag, D.P., 1998. A Neoproterozoic snowball earth. Science 281, 1342–1346.

Horwitz, E.P., Dietz, M.L., Fisher, D.E., 1991. Separation and preconcentration of strontium from biological, environmental, and nuclear waste samples by extraction chromatography using a crown-ether. Analytical Chemistry 63, 522–525.

Irwin, H., Curtis, C., Coleman, M., 1977. Isotopic evidence for source of diagenetic carbonates formed during burial of organic-rich sediments. Nature 269, 209–213.

Jackson, G.C.A., 1932. The geology of the Nchanga district, northern Rhodesia. Journal of the Geological Society, London 88, 443–515.

Jacobsen, S.B., Kaufman, A.J., 1999. The Sr, C, and O isotopic evolution of the Neoproterozoic seawater. Chemical Geology 161, 37–57.

John, T., Schenk, V., Mezger, K., Tembo, F., 2004. Timing and PT evolution of whiteschist metamorphism in the Lufilian arc – Zambezi belt orogeen (Zambia): implications for the assembly of Gondwana. Journal of Geology 122, 71–90.

Jordaan, J., 1961. Nkana. In: Mendelsohn, F. (Ed.), The Geology of the Northern Rhodesian Copperbelt. MacDonald, London, pp. 297–328.

Kampunzu, A.B., Cailteux, J., 1999. Tectonic evolution of the Lufilian Arc (Central African Copperbelt) during Neoproterozoic Pan African orogenesis. Gondwana Research 2, 401–421.

Kampunzu, A.B., Kapenda, D., Manteka, B., 1991. Basic magmatism and geotectonic evolution of the Pan African belt in central Africa: evidence from the Katangan and West Congolian segments. Tectonophysics 190, 363–371.

Kampunzu, A.B., Tembo, F., Matheis, G., Kapenda, D., Huntsman-Mapila, P., 2000. Geochemistry and tectonic setting of mafic igneous units in the Neoproterozoic Katangan Basin, Central Africa: implications for Rodinia break-up. Gondwana Research 3, 125–153.

Kelley, S.P., Fallick, A.E., 1990. A high precision spatially resolved analysis of δ^{34}S in sulphides using a laser extraction technique. Geochimica et Cosmochimica Acta 54, 883–888.

Kenis, I., Muchez, Ph., Verhaert, G., Boyce, A., Sintubin, M., 2005. Fluid evolution during burial and Variscan deformation in the Lower Devonian rocks of the high-Ardenne slate belt (Belgium): sources and causes of high-salinity and C–O–H–N fluids. Contributions to Mineralogy and Petrology 150, 102–118.

Key, R.M., Liyungu, A.K., Njamu, F.M., Somwe, V., Banda, J., Mosley, P.N., Armstrong, R.A., 2001. The western arm of the Lufilian Arc in NW Zambia and its potential for copper mineralisation. Journal of African Earth Sciences 33, 503–528.

Knoop, S.R., Kennedy, L.A., Dipple, G.M., 2002. New evidence for syntectonic fluid migration across the hinterland-foreland transition of the Canadian Cordillera. Journal of Geophysical Research 107, 2071–2098.

Lammens, L., 2009. Microthermometric and Isotope Study of the Nkana Cu–Co South Orebody, Zambia. Master Thesis in Geology, K.U. Leuven, Belgium, p. 93.

Lefebvre, J.-J., 1978. Le Groupe de Mwashya, mégacyclothème terminal de Roan (Shaba, Zaïre Sudoriental). I – Approche lithostratigraphique et étude de l'environnement sédimentaire. Annales de la Société Géologique de Belgique 101, 209–225.

Lerouge, C., Cailteux, J., Kampunzu, A.B., Milesi, J.P., Fléhoc, C., 2005. Sulphur isotope constraints on formation conditions of Luiswishi ore deposit, Democratic Republic of Congo (DRC). Journal of African Earth Sciences 42, 173–182.

Lindsay, J.F., Kruse, P.D., Green, O.R., Hawkins, E., Brasier, M.D., Cartlidge, J., Corfield, R.M., 2005. The Neoproterozoic–Cambrian record in Australia: a stable isotope study. Precambrian Research 143, 113–133.

Machel, H.G., Krouse, H.R., Sassen, R., 1995. Products and distinguishing criteria of bacterial and thermochemical sulfate reduction. Applied Geochemistry 10, 373–389.

Marquer, D., Burkhard, M., 1992. Fluid circulation, progressive deformation and mass-transfer processes in the upper crust: the example of basement–cover relationships in the External Crystalline Massifs, Switzerland. Journal of Structural Geology 14, 1047–1057.

McGowan, R.R., Roberts, S., Foster, R.P., Boyce, A.J., Coller, D., 2003. Origin of the copper–cobalt deposits of the Zambian Copperbelt: an epigenetic view from Nchanga. Geology 31, 497–500.

McGowan, R.R., Roberts, S., Boyce, A.J., 2006. Origin of the Nchanga copper–cobalt deposit of the Zambian Copperbelt. Mineralium Deposita 40, 617–638.

Mendelsohn, F., 1961. The Geology of the Northern Rhodesian Copperbelt. MacDonald, London. p. 523.

Muchez, Ph., Zhang, Y., Dejonghe, L., Viaene, W., Keppens, E., 1998. Evolution of palaeofluids at the Variscan thrust fromt in eastern Belgium. Geologische Rundschau 87, 373–380.

Muchez, Ph., Brems, D., El Desouky, H., Haest, M., Vanderhaeghen, P., Dewaele, S., Heijlen, W., Mukumba, W., 2007. Base metal ore deposit evolution and geodynamics in the Central African Copperbelt. In: Andrew et al. (Eds.) Digging Deeper. Proceedings of the 9th Biennial SGA Meeting, Dublin. Irish Association for Economic geology, Dublin (Ireland), pp. 213–216.

Muchez, Ph., Vanderhaeghen, P., El Desouky, H., Schneider, J., Boyce, A., Dewaele, S., Cailteux, J., 2008. Anhydrite pseudomorphs and the origin of stratiform Cu–Co ores in the Katangan Copperbelt (Democratic Republic of Congo). Mineralium Deposita 43, 575–589.

Ngoyi, K., Liégeois, J.-P., Demaiffe, D., Dumont, P., 1991. Age tardi-ubendien (Protérozoïque inférieur) des dômes granitiques de l'arc cuprifèrre zaïro-zambien. Compte Rendu de l'Académie des Sciences de Paris 313, 83–89.

Northrop, D.A., Clayton, R.N., 1966. Oxygen isotope fractionations in systems containing dolomite. Journal of Geology 74, 174–196.

Philpotts, A.R., Ague, J.J., 2009. Principles of Igneous and Metamorphic Petrology. Cambridge University Press, Cambridge. 667 p.

Porada, H., 1989. Pan-African rifting and orogenesis on Southern to Equatorial Africa and Eastern Brazil. Precambrian Research 44, 103–136.

Porada, H., Berhorst, V., 2000. Towards a new understanding of the Neoproterozoic – early Paleozoic Lufilian and northern Zambezi belts in Zambia and the Democratic Republic of Congo. Journal of African Earth Sciences 30, 727–771.

Rainaud, C., Master, S., Armstrong, R.A., Philipps, D., Robb, L.J., 2005. Monazite dating and ^{40}Ar–^{39} Ar thermochronology of metamorphic events in the Central African Copperbelt during the Pan-African Lufilian Orogeny. Journal of African Earth Sciences 42, 183–199.

Roberts, S., Palmer, M.R., Cooper, M.J., Buchaus, P., Sargent, D., 2009. REE and Sr isotope characteristics of carbonate within the Cu–Co mineralized sedimentary sequence of the Nchanga Mine, Zambian Copperbelt. Mineralium Deposita 44, 881–891.

Roedder, E., 1984. Fluid inclusions. Reviews in Mineralogy, vol. 12. Mineralogical Society of America. p. 646.

Rosenbaum, J., Sheppard, S.M., 1986. An isotopic study of siderites, dolomites and ankerites at high temperatures. Geochimica et Cosmochimica Acta 50, 1147–1150.

Selley, D., Broughton, D., Scott, R., Hitzman, M., Bull, S., Large, McGoldrick, P., Croaker, M., Pollington, N., Barra, F., 2005. A New Look at the Geology of the Zambian Copperbelt. Economic Geology 100th Anniversary Volume, Society of Economic Geology, Tulsa, pp. 965–1000.

Shepherd, T.J., Rankin, A.H., Alderton, D.H.M., 1985. A Practical Guide to Fluid Inclusion Studies. Blackie and Son, New York. p. 239.

Sheppard, S.M.F., 1986. Characterization and isotopic variations in natural waters. In: Valley, J.W., Taylor, H.P., O'Neil, J.R. (Eds.), Stable Isotopes in High Temperature Geological Processes. Reviews in Mineralogy 16, 165–183.

Sibson, R.H., 2001. Seismogenic framework for hydrothermal transport and ore deposition. Society of Economic Geologists Reviews 14, 25–50.

Sweeney, M.A., Binda, P.L., 1989. The role of diagenesis in the formation of the Konkola Cu–Co orebody of the Zambian Copperbelt. In: Boyle, R.W., Brown, A.C., Jeferson, C.W., Jowett, E.C., Kirkham, R.V. (Eds.), Sediment-Hosted Stratiform Copper Deposits. Geological Association of Canada, Special Paper 36, pp. 499–518.

Sweeney, M.A., Turner, P., Vaughan, D.J., 1986. Stable isotope and geochemical studies of the role of early diagenesis in ore formation, Ko, kola basin, Zambian Copperbelt. Economic Geology 81, 1838–1852.

Thirlwall, M.F., 1991. Long-term reproducibility of multicollector Sr and Nd isotope ratio analysis. Chemical Geology 94, 85–104.

Unrug, R., 1988. Mineralization controls and source of metals in the Lufilian fold belt, Shaba (Zaire), Zambia and Angola. Economic Geology 83, 1247–1258.

Veizer, J., Hoefs, J., 1976. The nature of $^{18}O/^{16}O$ and $^{13}C/^{12}C$ secular trends in sedimentary carbonate rocks. Geochimica et Cosmochimica Acta 40, 1387–1395.

Wachter, E., Hayes, J.M., 1985. Exchange of oxygen isotopes in carbon-dioxide – phosphoric acid systems. Chemical Geology 52, 365–374.

Wendorff, M., 2002. Stratigraphy of the Fungurume group-evolving foreland basin succession in the Lufilian fold-thrust belt, Neoproterozoic–Lower Palaeozoic, Democratic Republic of Congo. South African Journal of Geology 106, 47–64.

Wendorff, M., 2005. Sedimentary genesis and lithostratigraphy of Neoproterozoic megabreccia from Mufulira, Copperbelt of Zambia. Journal of African Earth Sciences 42, 61–81.